Discrete unified gas-kinetic wave-particle method for flows in all flow regimes

L. M. Yang,[1,2,3,*] Z. H. Li,[4,5,†] C. Shu,[6] Y. Y. Liu,[6] W. Liu,[6] and J. Wu[1,2,3]

[1]*State Key Laboratory of Mechanics and Control for Aerospace Structures, Nanjing University of Aeronautics and Astronautics, Nanjing 210016, China*

[2]*MIIT Key Laboratory of Unsteady Aerodynamics and Flow Control, Nanjing University of Aeronautics and Astronautics, Nanjing 210016, China*

[3]*Department of Aerodynamics, College of Aerospace Engineering, Nanjing University of Aeronautics and Astronautics, Nanjing 210016, China*

[4]*Hypervelocity Aerodynamics Institute, China Aerodynamics Research and Development Center, Mianyang 621000, China*

[5]*National Laboratory for Computational Fluid Dynamics, Beihang University, Beijing 100191, China*

[6]*Department of Mechanical Engineering, National University of Singapore, Singapore 117576, Singapore*

(Received 13 February 2023; accepted 16 June 2023; published 14 July 2023)

This work proposes a discrete unified gas-kinetic wave-particle (DUGKWP) method for simulation of flows in all flow regimes. Unlike the discrete velocity method (DVM) and the direct simulation Monte Carlo (DSMC) method which solve the governing equations by either the deterministic method or the stochastic method, the DUGKWP combines the advantages of these two methods. In the DUGKWP, the information of microscopic particles as well as macroscopic flow variables are both evolved. Specifically, the microscopic particles are updated by the free-transport and resampling processes, while the macroscopic flow properties are evolved via solving the macroscopic governing equations of conservation laws with the finite volume method. According to the discrete characteristic solution to the Boltzmann-BGK equation utilized in the DUGKWP, in the highly rarefied flow regime, the motion of microscopic particles greatly determines the fluxes for the macroscopic governing equations. Conversely, for the continuum flow, no microscopic particle exists in the computational domain and the DUGKWP is degraded to the Navier-Stokes solver. Numerical studies validate that the DUGKWP can accurately predict the flow properties in all flow regimes. Furthermore, compared with the deterministic method, the DUGKWP enjoys superior efficiency with less memory consumption for both high-speed rarefied flows and flows close to the continuum regime.

DOI: 10.1103/PhysRevE.108.015302

I. INTRODUCTION

The rarefaction of fluid flows is characterized by the ratio of the molecular mean-free path to the characteristic length, namely, the Knudsen (Kn) number. In fact, the commonly used Navier-Stokes (N-S) equations can be applied only for the continuum flow (Kn < 0.001) due to the dependence on the continuum assumption. Different from the N-S equations, the Boltzmann equation is not limited to the continuum assumption. It provides the possibility for simulation of fluid flow problems from the free molecular to the continuum flow regime by solving the Boltzmann equation. Generally, the methods for solving the Boltzmann equation can be categorized into two types: the stochastic methods [1–5] and the deterministic methods [6–10]. Both have their strengths, but also some weaknesses.

As one representative stochastic method, the direct simulation Monte Carlo (DSMC) approach was first proposed by Bird [11], which uses a probabilistic simulation to solve the Boltzmann equation. In this method, the real gas atoms or molecules are represented by the simulation particles, and the gas physics is described by the decoupling of the motion of particles from their collisions. Since the velocity of the particle is correlated with the local mean flow velocity, it is equivalent to the adaptive distribution in the molecular velocity space. Given this, the DSMC method enjoys excellent efficiency in the simulation of supersonic/hypersonic rarefied flow problems [12,13], in which the variation range of the mean flow velocity in the whole computational domain is very large. However, due to the decoupling of the motion and collision processes in the DSMC method, the typical cell size and the time-step size are subject to values smaller than the mean-free path and the mean collision time of the gas molecules, respectively. These requirements limit the application of DSMC method in the simulation of the continuum and near-continuum flows where the mean-free path and collision time of the gas molecules are particularly small. To overcome this defect, the hybrid N-S/DSMC method was developed [14–16]. This method divides the computational domain into the continuum region and the rarefied region first based on the local Kn number, then the N-S solver is utilized in the continuum region while the DSMC method is applied in the rarefied region. As a result, the efficiency of the DSMC simulation in the continuum region can be improved. However, the hybrid method usually needs to introduce a buffer zone, and the numerical results are sensitive to the location of the division plane between the two computational regions as commented by Torre [17].

*Corresponding author: lmyang@nuaa.edu.cn
†Corresponding author: zhli0097@x263.net

Different from the DSMC method, the discrete velocity method (DVM) solves the Boltzmann equation by discretizing it in both the physical space and the molecular velocity space. It belongs to the deterministic methods. To simplify the calculation of the DVM, the collisional integral term in the original Boltzmann equation is generally replaced by some simplified models, such as the BGK model [18] and BGK-Shakhov model [19]. Within the DVM framework, various approaches have been proposed to resolve the fluid flow problems in all flow regimes [20–24]. By solving the discrete velocity Boltzmann equation (DVBE) with the nonoscillatory nonfree dissipative (NND) scheme, the gas-kinetic unified algorithm (GKUA) was developed by Li and Zhang [25,26]. Xu and Huang [27] developed the unified gas-kinetic scheme (UGKS) by introducing the local integral solution to the Boltzmann-BGK equation to calculate the numerical fluxes of the DVBE and the corresponding macroscopic governing equations. Zhu *et al.* [28] further extended the UGKS to the unsteady scenario. Guo *et al.* [29,30] put forward the discrete unified gas-kinetic scheme (DUGKS) which applies the local discrete characteristic solution to the Boltzmann-BGK equation to calculate the numerical fluxes of the DVBE, and then Liu *et al.* [31] proposed the conserved DUGKS where both the DVBE and the corresponding macroscopic governing equations are solved. In addition, Yang *et al.* [32,33] proposed the improved discrete velocity method (IDVM) by considering the collision effect in the calculation of numerical fluxes of the macroscopic governing equations while using the local solution to the collisionless Boltzmann equation to evaluate the numerical fluxes of the DVBE. By virtue of the coupling of the motion and collision processes, the UGKS, DUGKS, and IDVM can provide accurate results from the continuum to the free molecular flow regime without the limitations that the sizes of the mesh and the time step should be smaller than the mean-free path and the mean collision time of the gas molecules. Nevertheless, the discretization in the molecular velocity space will seriously increase the computational cost and the required virtual memory of these DVMs, especially when high-speed flows are considered.

Recently, to retain the high efficiency of the DSMC method for simulation of supersonic or hypersonic rarefied flows and the accuracy of the UGKS in all flow regimes, the unified gas-kinetic wave-particle (UGKWP) method was proposed by Liu *et al.* [34]. In the UGKWP, the gas physics is captured by both the deterministic hydrodynamic waves and the stochastic microscopic particles, and their respective contributions are dependent on the ratio of time-step size to local collision time. In the highly rarefied flow regime, the stochastic microscopic particles dominate the solution and the UGKWP recovers nonequilibrium flow physics by the free-transport process of particles. In the continuum flow regime, the deterministic hydrodynamic waves dominate the solution and the UGKWP reduces to the gas-kinetic scheme (GKS) for the N-S equations. Correspondingly, the evolution of discrete distribution functions is avoided and the number of microscopic particles is adaptively controlled by the ratio of time-step size to local collision time. As a result, the UGKWP provides efficient and accurate simulations not only for the supersonic/hypersonic rarefied flows but also for the continuum flows. Subsequently, Zhu *et al.* [35] extended the UGKWP to the unstructured mesh for fluid flow problems involving curved boundaries. Chen *et al.* [36] further extended the UGKWP to the three-dimensional scenario and validated its performance by simulating the hypersonic flow over a space vehicle. Liu *et al.* [37] developed a simplified unified wave-particle method with the quantified model-competition mechanism based on the UGKWP.

In this paper, inspired by the idea of the UGKWP, a discrete unified gas-kinetic wave-particle (DUGKWP) method is proposed to effectively simulate flows in all flow regimes. First, a modified DUGKS is developed by applying the discrete characteristic solution to the Boltzmann-BGK equation for evaluating the numerical fluxes of both the DVBE and the corresponding macroscopic governing equations. Then the discrete characteristic solution is further used to model the contributions of the hydrodynamic waves and the microscopic particles in the DUGKWP. Like the UGKWP, both the information of microscopic particles and macroscopic flow quantities are evolved in the DUGKWP. Specifically, the microscopic particles are updated by the free-transport and resampling processes, and the macroscopic flow variables are evolved through solving the macroscopic governing equations of conservation laws with the finite volume method. In particular, the macroscopic numerical fluxes at the cell interface are calculated by both the hydrodynamic waves and the microscopic particles. According to the discrete characteristic solution to the Boltzmann-BGK equation, in the highly rarefied flow regime, the macroscopic fluxes are mainly attributed to the motion of microscopic particles, while in the continuum flow regime, no microscopic particle exists in the computational domain and the DUGKWP is reduced to the N-S solver. The performance of the DUGKWP will be investigated by several one-dimensional and two-dimensional numerical tests from the continuum to the free molecular flow regime, and the results will be compared with the modified DUGKS as well as the UGKS.

II. MODIFIED DISCRETE UNIFIED GAS-KINETIC SCHEME

Different from the original DUGKS [29], in which only the DVBE is resolved, the modified DUGKS solves the DVBE as well as the corresponding macroscopic governing equations. In this work, we confine the study to the Boltzmann-BGK equation for simplicity, which has the following form:

$$\frac{\partial f}{\partial t} + \boldsymbol{\xi} \cdot \nabla f = \Omega \equiv \frac{g - f}{\tau}, \tag{1}$$

where $\boldsymbol{\xi}$ is the molecular velocity vector, Ω represents the collision operator, and τ denotes the collision time. f is the distribution function, and g is its equilibrium state, which is defined by the Maxwellian distribution function

$$g = \frac{\rho}{(2\pi R_g T)^{3/2}} \exp\left(-\frac{c^2}{2R_g T}\right), \tag{2}$$

where ρ denotes the density, T denotes the temperature, $\mathbf{c} = \boldsymbol{\xi} - \mathbf{u}$ represents the molecular thermal velocity vector, $\mathbf{u}$ denotes the mean flow velocity, $c = |\mathbf{c}|$ refers to the magnitude of $\mathbf{c}$, and R_g denotes the gas constant.

According to the relationship between the distribution function and the macroscopic flow variables, the corresponding macroscopic governing equations to Eq. (1) can be obtained as follows:

$$\frac{\partial \mathbf{W}}{\partial t} + \nabla \cdot \mathbf{F} = \mathbf{0} \tag{3}$$

with the conservative flow variable vector $\mathbf{W}$ and the flux vector $\mathbf{F}$ computed by

$$\mathbf{W} = (\rho, \rho\mathbf{u}, \rho E)^T = \langle \boldsymbol{\psi} f \rangle, \tag{4}$$

$$\mathbf{F} = (F_\rho, F_{\rho\mathbf{u}}, F_{\rho E})^T = \langle \boldsymbol{\xi}\boldsymbol{\psi} f \rangle. \tag{5}$$

Here $\boldsymbol{\psi} = (1, \boldsymbol{\xi}, \xi^2/2)^T$ is the moment vector and $\xi = |\boldsymbol{\xi}|$ is the magnitude of $\boldsymbol{\xi}$. The notation $\langle f \rangle = \int f d\boldsymbol{\xi}$ defines the integral of the distribution function in the entire velocity space. Note that the compatibility condition has been utilized in Eq. (3).

A. Solution of discrete velocity Boltzmann equation

In the framework of the DVM, Eq. (1) is first discretized in the velocity space

$$\frac{\partial f_\alpha}{\partial t} + \boldsymbol{\xi}_\alpha \cdot \nabla f_\alpha = \Omega_\alpha = \frac{g_\alpha - f_\alpha}{\tau}, \quad \alpha = 1, \ldots, N_V, \tag{6}$$

where N_V and the subscript α are the total number of discrete velocity points and the index in the discrete velocity space, respectively. Integrating Eq. (6) over a control volume V_i and a time interval $[0, \Delta t]$, we can obtain

$$f_{i,\alpha}^{n+1} - f_{i,\alpha}^{n} + \frac{1}{V_i}\sum_{j\in N(i)} S_{ij}\int_0^{\Delta t} \mathbf{n}_{ij}\cdot\boldsymbol{\xi}_\alpha f_{ij,a}(t)dt = \int_0^{\Delta t}\Omega_\alpha dt. \tag{7}$$

Here the superscripts n and $n+1$ represent the current time step and the new time step, respectively. $N(i)$ is the set of neighboring cells of the cell i. $\mathbf{n}_{ij}$ denotes the outward unit normal vector. S_{ij} is the area of the interface shared by the cells i and j. Δt is the time-step size, which is determined by the Courant-Friedrichs-Lewy (CFL) condition. Applying the trapezoidal law to the right-hand side of Eq. (7), we can obtain the explicit evolution equation of the discrete distribution function as follows:

$$f_{i,\alpha}^{n+1} = \frac{2\tau_i^{n+1}}{2\tau_i^{n+1}+\Delta t}\left[f_{i,\alpha}^{n} - \frac{1}{V_i}\sum_{j\in N(i)} S_{ij}\int_0^{\Delta t}\mathbf{n}_{ij}\cdot\boldsymbol{\xi}_\alpha f_{ij,a}(t)dt + \frac{\Delta t}{2}\left(\frac{g_{i,\alpha}^{n} - f_{i,\alpha}^{n}}{\tau_i^{n}} + \frac{\bar{g}_{i,\alpha}^{n+1}}{\tau_i^{n+1}}\right)\right]. \tag{8}$$

As shown in Eq. (8), the evolution of the distribution function requires the calculation of the equilibrium state at the new time level $\bar{g}_{i,\alpha}^{n+1}$ and the discrete distribution function at the cell interface $f_{ij,a}(t)$. $\bar{g}_{i,\alpha}^{n+1}$ is the function of the macroscopic variables, which can be predicted from the solution of Eq. (3) like the UGKS [27,28] and IDVM [32,33]. The calculation of $\bar{g}_{i,\alpha}^{n+1}$ will be illustrated in Sec. II B. As for the discrete distribution function $f_{ij,a}(t)$, it can be obtained from the characteristic solution to the Boltzmann-BGK Eq. (1) at the cell interface

$$f_{ij}(t) \equiv f(\mathbf{x}_{ij}, t) = f(\mathbf{x}_{ij} - \boldsymbol{\xi}t, 0) + \frac{t}{2}[\Omega(\mathbf{x}_{ij} - \boldsymbol{\xi}t, 0) + \Omega(\mathbf{x}_{ij}, t)], \tag{9}$$

where $\mathbf{x}_{ij}$ represents the location at the cell interface. Equation (9) can be rearranged as

$$f(\mathbf{x}_{ij}, t) = \frac{2\tau - t}{2\tau + t} f(\mathbf{x}_{ij} - \boldsymbol{\xi}t, 0) + \frac{t}{2\tau + t}[g(\mathbf{x}_{ij} - \boldsymbol{\xi}t, 0) + g(\mathbf{x}_{ij}, t)]. \tag{10}$$

Similar to the original DUGKS [29], the discretization in the molecular velocity space is introduced into Eq. (10), and the rectangular rule is adopted to calculate the numerical fluxes in Eq. (8), which yields

$$\int_0^{\Delta t} \mathbf{n}_{ij}\cdot\boldsymbol{\xi}_\alpha f_{ij,a}(t)dt \approx \Delta t\,\mathbf{n}_{ij}\cdot\boldsymbol{\xi}_\alpha f_{ij,a}(h), \tag{11}$$

$$f_{ij,a}(h) = \frac{2\tau - h}{2\tau + h} f_a(\mathbf{x}_{ij} - \boldsymbol{\xi}_\alpha h, 0) + \frac{h}{2\tau + h}[g_\alpha(\mathbf{x}_{ij} - \boldsymbol{\xi}_\alpha h, 0) + g_\alpha(\mathbf{x}_{ij}, h)], \tag{12}$$

Here $h = \Delta t/2$ is the half-time-step size. The discrete distribution function $f_a(\mathbf{x}_{ij} - \boldsymbol{\xi}_\alpha h, 0)$ and its equilibrium state $g_\alpha(\mathbf{x}_{ij} - \boldsymbol{\xi}_\alpha h, 0)$ at the surrounding point of the cell interface at the current time level can be interpolated from those at the cell center. To evaluate the discrete equilibrium state at the cell interface $g_\alpha(\mathbf{x}_{ij}, h)$, we first apply the compatibility condition to Eq. (12), which yields

$$\mathbf{W}(\mathbf{x}_{ij}, h) = \frac{2\tau - h}{2\tau}\langle \boldsymbol{\psi} f_a(\mathbf{x}_{ij} - \boldsymbol{\xi}_\alpha h, 0)\rangle_a + \frac{h}{2\tau}\langle \boldsymbol{\psi} g_a(\mathbf{x}_{ij} - \boldsymbol{\xi}_\alpha h, 0)\rangle_a. \tag{13}$$

Then $g_\alpha(\mathbf{x}_{ij}, h)$ can be obtained by substituting $\mathbf{W}(\mathbf{x}_{ij}, h)$ into Eq. (2). Note that the integral in Eq. (13) should be replaced by the numerical quadrature considering the discretization in the molecular velocity space. It has been distinguished from the analytical integration with the subscript "α."

B. Solution of macroscopic governing equations

To predict $\bar{g}_{i,\alpha}^{n+1}$, the macroscopic governing equation (3) should be solved. By explicitly discretizing Eq. (3) over a control volume V_i, we have

$$\overline{\mathbf{W}}_i^{n+1} - \mathbf{W}_i^{n} + \frac{\Delta t}{V_i}\sum_{j\in N(i)} S_{ij}\mathbf{n}_{ij}\cdot\mathbf{F}_{ij} = \mathbf{0}. \tag{14}$$

According to the definition of macroscopic fluxes (5) and using the rectangular rule to approximate the time integration over $[0, \Delta t]$, we can obtain

$$\mathbf{F}_{ij} = \frac{1}{\Delta t}\left\langle \int_0^{\Delta t} \boldsymbol{\xi}_\alpha\boldsymbol{\psi} f_{ij,a}(t)dt\right\rangle_\alpha \approx \langle \boldsymbol{\xi}_\alpha\boldsymbol{\psi} f_{ij,a}(h)\rangle_\alpha. \tag{15}$$

Since $f_{ij,a}(h)$ has been determined by Eq. (12), $\overline{\mathbf{W}}_i^{n+1}$ can be obtained easily by Eq. (15). Then $\bar{g}_{i,\alpha}^{n+1}$ can be calculated by substituting $\overline{\mathbf{W}}_i^{n+1}$ into Eq. (2).

It can be seen from the above derivation that the modified DUGKS shares some common features with the original DUGKS, such as the use of the trapezoidal law to approximate the collision term and the rectangular rule to approximate the time integral of numerical fluxes at the cell interface. However, the modified DGUKS solves both the DVBE and its corresponding macroscopic governing equations simultaneously, and the transformations of discrete distribution functions used in the original DUGKS are avoided. As commented by Liu *et al.* [38] and Chen *et al.* [39], the introduction of the macroscopic governing equations to predict the equilibrium state at the new time level leads to better performance on the conservativeness than the original DUGKS.

III. DISCRETE UNIFIED GAS-KINETIC WAVE-PARTICLE METHOD

As we know, the conservation laws of the mass, momentum, and energy in a control volume within a time step are fundamental for resolving the fluid flow problems on the scale of mesh size and time-step size. The multiscale flow evolution in the above DUGKS relies on the reconstruction of numerical fluxes at the cell interface by coupling the motion of particles from their collisions. This is realized by the local characteristic solution to the Boltzmann-BGK equation. The DUGKWP will also be designed from this local solution, which can be rewritten as

$$f(\mathbf{x}_{ij},t_e)=\underbrace{\frac{2\tau-t_e}{2\tau+t_e}f(\mathbf{x}_{ij}-\boldsymbol{\xi}t_e,0)}_{f_{ij}^{fr}(t_e)}+\underbrace{\frac{t_e}{2\tau+t_e}[g(\mathbf{x}_{ij}-\boldsymbol{\xi}t_e,0)+g(\mathbf{x}_{ij},t_e)]}_{f_{ij}^{eq}(t_e)},\quad(16)$$

where t_e is the scale-dependent observation time. $f_{ij}^{fr}(t_e)$ and $f_{ij}^{eq}(t_e)$ are related to the evolution of the initial distribution function and the local equilibrium state, respectively. More specifically, $f_{ij}^{fr}(t_e)$ and $f_{ij}^{eq}(t_e)$ are contributed to the free-streaming fluxes and the equilibrium fluxes, respectively. Equation (16) shows that in a time interval $[0,t_e]$, there is a $(2\tau-t_e)/(2\tau+t_e)$ portion of particles without suffering collision, and the other particles suffer at least one collision. If $t_e=2\tau$, all particles will collide with other particles in a time interval $[0,t_e]$ and the flow field can be regarded as the continuous flow. When $t_e>2\tau$, the ratio of particles without suffering collision becomes negative. This situation is unphysical, and it can also be treated as the continuum flow directly.

In the modified DUGKS, the distribution function is further discretized in the molecular velocity space to calculate the numerical fluxes and evolve the distribution function itself as well as the macroscopic conservative variables. But, in fact, the numerical fluxes for updating the macroscopic conservative variables can also be evaluated by the deterministic hydrodynamic waves and the stochastic microscopic particles. This strategy has been utilized in the UGKWP [34,35]. In this section, a multiscale DUGKWP will be constructed by applying Eq. (16).

A. Calculation of equilibrium fluxes

When introducing the microscopic particles to evaluate the free-streaming fluxes, the discretization in the molecular velocity space can be avoided and the nonequilibrium effect can be captured by tracking the microscopic particles. In this way the evolution of the macroscopic flow variables [Eq. (14)] can be rewritten as

$$\mathbf{W}_i^{n+1}=\mathbf{W}_i^n-\frac{\Delta t}{V_i}\sum_{j\in N(i)}S_{ij}\mathbf{n}_{ij}\cdot\mathbf{F}_{ij}^{eq}+\frac{\mathbf{F}_i^{fr}}{V_i},\quad(17)$$

where $\mathbf{F}_{ij}^{eq}$ and $\mathbf{F}_i^{fr}$ are the macroscopic fluxes attributed to $f_{ij}^{eq}(t_e)$ and $f_{ij}^{fr}(t_e)$, respectively. In the DUGKWP, $\mathbf{F}_i^{fr}$ are calculated analytically from the hydrodynamic waves and by counting the particles across the cell interface, which will be elaborated in Sec. III B, and $\mathbf{F}_{ij}^{eq}$ are computed by substituting $f_{ij}^{eq}(t_e)$ into Eq. (5) and integrating over a time interval $[0,\Delta t]$ directly. But in the calculation of $\mathbf{F}_{ij}^{eq}$, two circumstances need to be considered according to the ratio of particles without suffering collision, $\beta=(2\tau-\Delta t)/(2\tau+\Delta t)$, where the scale-dependent observation time t_e has been taken as the time-step size Δt.

Case A: $\Delta t<2\tau$, the particle's free transport needs to be considered. In this case, the ratio of particles without suffering collision is positive, both $f_{ij}^{eq}(t_e)$ and $f_{ij}^{fr}(t_e)$ contribute to the evaluation of macroscopic fluxes. Thus, $\mathbf{F}_{ij}^{eq}$ can be calculated

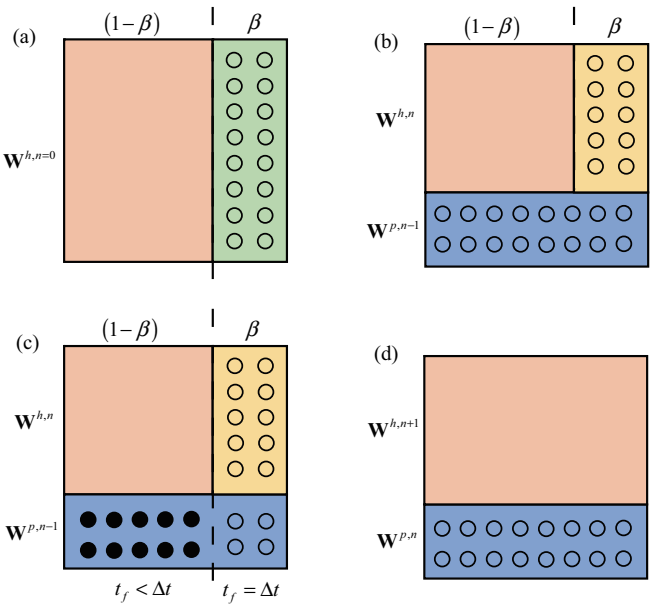

FIG. 1. Time evolution of microscopic particles and macroscopic flow variables in the DUGKWP method. (a) Initial field for the first step; (b) initial field for the nth step; (c) classification of collisionless (white circle) and collisional particles (solid circle) for $\mathbf{W}^{p,n-1}$; (d) update on both the microscopic and macroscopic levels.

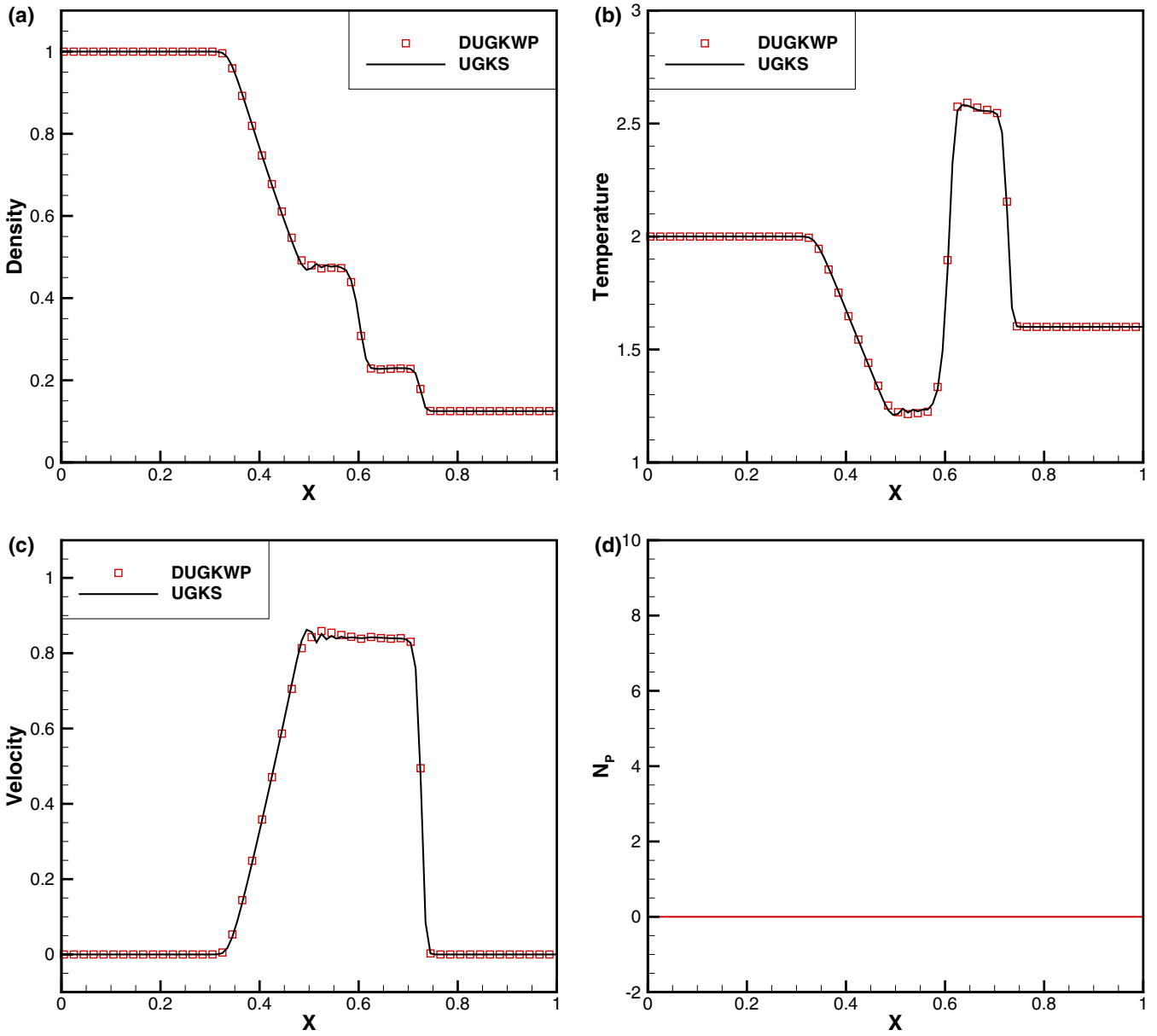

FIG. 2. Distributions of density, temperature, velocity, and number of simulation particles for Sod shock tube problem at $\mu_{\text{ref}} = 10^{-5}$. (a) Density; (b) temperature; (c) velocity; (d) number of simulation particles.

by integrating $f_{ij}^{eq}(t_e)$ over a time interval $[0, \Delta t]$ and substituting the resultant equation into Eq. (5) directly:

$$\mathbf{F}_{ij}^{eq} = \frac{1}{\Delta t}\left\langle \boldsymbol{\xi}\boldsymbol{\psi}\int_0^{\Delta t} f_{ij}^{eq}(t_e)dt_e \right\rangle, \tag{18}$$

For ease of calculation of the above integration and to achieve the second order of accuracy, the terms in $f_{ij}^{eq}(t_e)$ can be expanded as

$$g(\mathbf{x}_{ij} - \boldsymbol{\xi}t_e, 0) = \begin{cases} g^L(\mathbf{x}_{ij}, 0) - t_e\boldsymbol{\xi}\cdot\nabla g(\mathbf{x}_i, 0), & \mathbf{n}_{ij}\cdot\boldsymbol{\xi} \geqslant 0 \\ g^R(\mathbf{x}_{ij}, 0) - t_e\boldsymbol{\xi}\cdot\nabla g(\mathbf{x}_j, 0), & \mathbf{n}_{ij}\cdot\boldsymbol{\xi} < 0 \end{cases}, \tag{19}$$

$$g(\mathbf{x}_{ij}, t_e) = g(\mathbf{x}_{ij}, 0) + t_e\partial_t g(\mathbf{x}_{ij}, 0), \tag{20}$$

where $\mathbf{x}_i$ and $\mathbf{x}_j$ represent the coordinates of cell centers of the left and right cells, respectively. $g^L(\mathbf{x}_{ij}, 0)$ and $g^R(\mathbf{x}_{ij}, 0)$ denote the interfacial states of the initial equilibrium distribution functions at the left and right sides. They can be computed from the macroscopic flow variables at the corresponding positions which are reconstructed from those at cell centers with a slope limiter function. $g(\mathbf{x}_{ij}, 0)$ is the equilibrium distribution function at the cell interface, which can be calculated by the following compatibility condition:

$$\begin{aligned}\mathbf{W}(\mathbf{x}_{ij}, 0) &= \langle \boldsymbol{\psi} g(\mathbf{x}_{ij}, 0)\rangle \\ &= \langle \boldsymbol{\psi} g^L(\mathbf{x}_{ij}, 0)\rangle_{>0} + \langle \boldsymbol{\psi} g^R(\mathbf{x}_{ij}, 0)\rangle_{<0}.\end{aligned} \tag{21}$$

Here the notations $\langle\cdot\rangle_{>0}$ and $\langle\cdot\rangle_{<0}$ define the integrations in the half left and half right velocity space, respectively. In addition, the spatial derivatives of the initial equilibrium distribution function at the cell centers of the left and right cells ($\nabla g(\mathbf{x}_i, 0)$ and $\nabla g(\mathbf{x}_j, 0)$) and the time derivative of

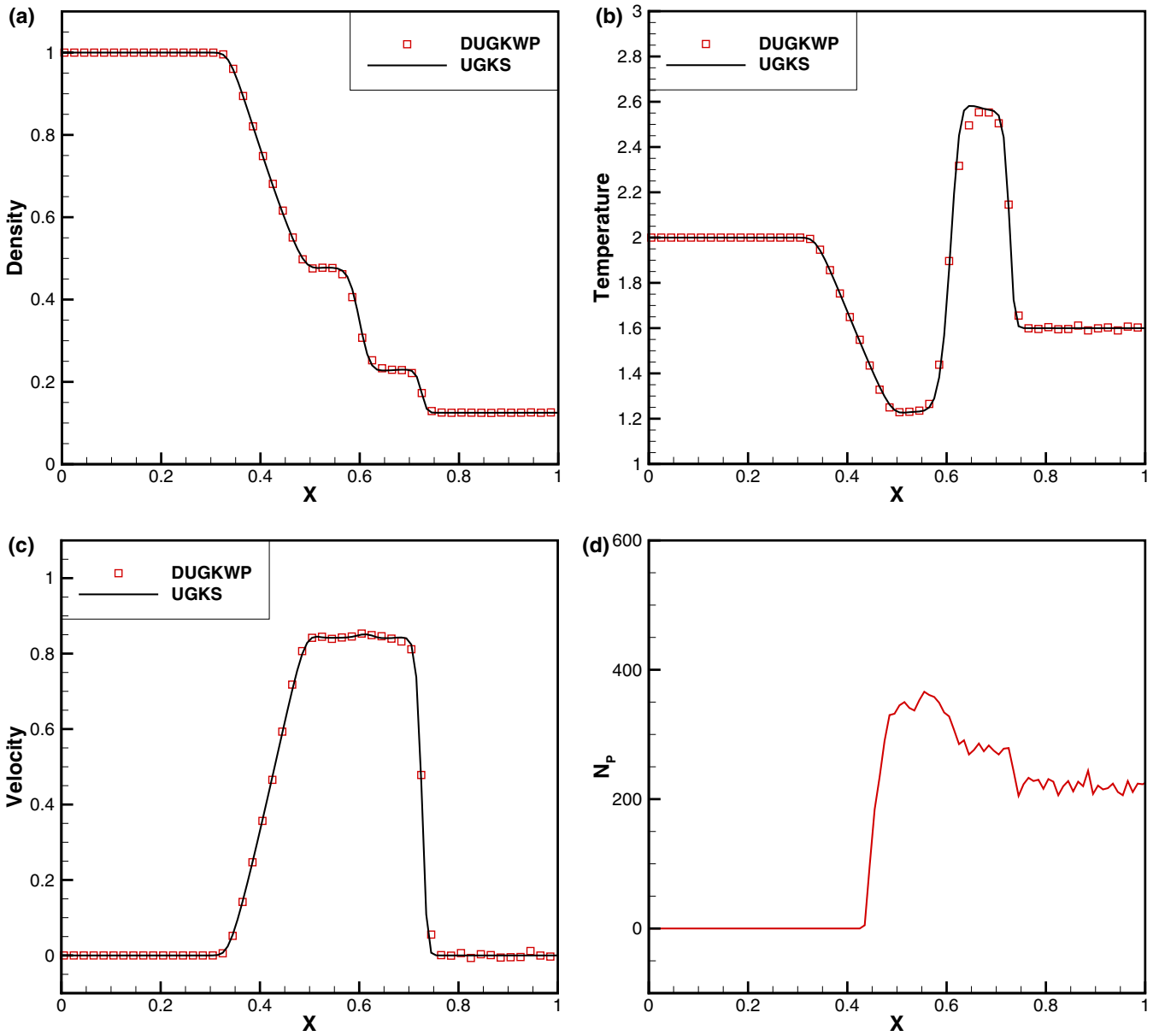

FIG. 3. Distributions of density, temperature, velocity, and number of simulation particles for Sod shock tube problem at $\mu_{\text{ref}} = 10^{-4}$. (a) Density; (b) temperature; (c) velocity; (d) number of simulation particles.

the equilibrium distribution function at the cell interface $\partial_t g(\mathbf{x}_{ij}, 0)$ can be obtained by the following micro-macro relationships:

$$\nabla \mathbf{W}(\mathbf{x}_i, 0) = \langle \boldsymbol{\psi} \nabla g(\mathbf{x}_i, 0) \rangle, \quad \nabla \mathbf{W}(\mathbf{x}_j, 0) = \langle \boldsymbol{\psi} \nabla g(\mathbf{x}_j, 0) \rangle, \tag{22}$$

$$\langle \boldsymbol{\psi} \partial_t g(\mathbf{x}_{ij}, 0) \rangle = -[\langle \boldsymbol{\psi} \boldsymbol{\xi} \cdot \nabla g(\mathbf{x}_i, 0) \rangle_{>0} + \langle \boldsymbol{\psi} \boldsymbol{\xi} \cdot \nabla g(\mathbf{x}_j, 0) \rangle_{<0}]. \tag{23}$$

The detailed expressions of Eqs. (22) and (23) can be found in Ref. [40]. Note that the introducing of the discontinuity of initial equilibrium distribution functions and their derivatives at the cell interface is to enhance the numerical stability.

Substituting Eqs. (19) and (20) into the expression of $f_{ij}^{eq}(t_e)$ and using the rectangular rule to approximate the time integration over $[0, \Delta t]$, we can get

$$\begin{aligned} \int_0^{\Delta t} f_{ij}^{eq}(t_e) dt_e = {} & c_1 \{ g(\mathbf{x}_{ij}, 0) + H(\mathbf{n}_{ij} \cdot \boldsymbol{\xi}) g^L(\mathbf{x}_{ij}, 0) \\ & + [1 - H(\mathbf{n}_{ij} \cdot \boldsymbol{\xi})] g^R(\mathbf{x}_{ij}, 0) \} \\ & + c_2 \{ \partial_t g(\mathbf{x}_{ij}, 0) - H(\mathbf{n}_{ij} \cdot \boldsymbol{\xi}) \boldsymbol{\xi} \cdot \nabla g(\mathbf{x}_i, 0) \\ & - [1 - H(\mathbf{n}_{ij} \cdot \boldsymbol{\xi})] \boldsymbol{\xi} \cdot \nabla g(\mathbf{x}_j, 0) \} \end{aligned} \tag{24}$$

where

$$c_1 = \frac{h \Delta t}{2\tau + h}, \quad c_2 = h c_1. \tag{25}$$

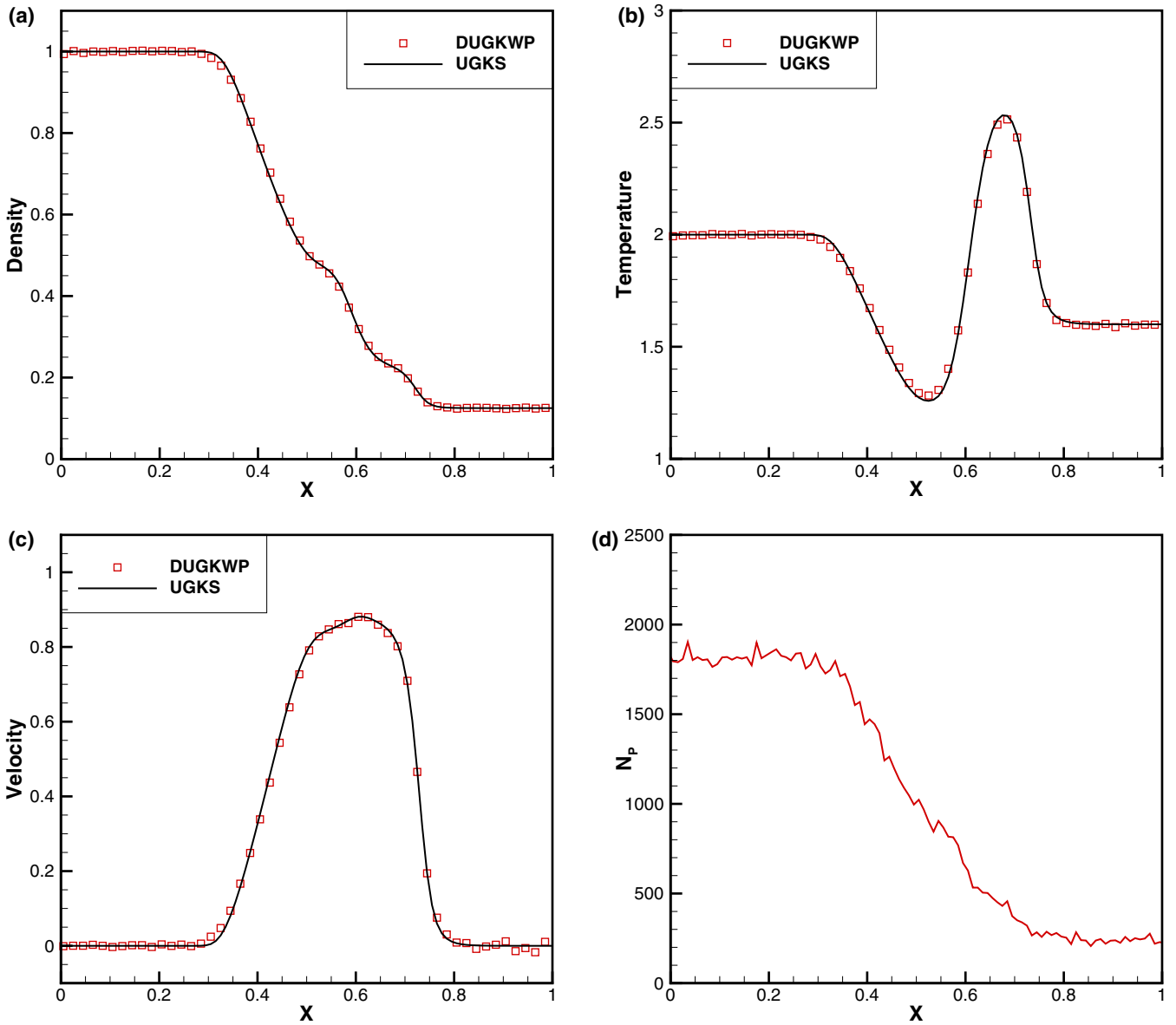

FIG. 4. Distributions of density, temperature, velocity, and number of simulation particles for Sod shock tube problem at $\mu_{\text{ref}} = 10^{-3}$. (a) Density; (b) temperature; (c) velocity; (d) number of simulation particles.

In addition, $H(\mathbf{n}_{ij} \cdot \boldsymbol{\xi})$ is the Heaviside function, $H(\mathbf{n}_{ij} \cdot \boldsymbol{\xi}) = 1$ for $\mathbf{n}_{ij} \cdot \boldsymbol{\xi} \geqslant 0$ and $H(\mathbf{n}_{ij} \cdot \boldsymbol{\xi}) = 0$ for $\mathbf{n}_{ij} \cdot \boldsymbol{\xi} < 0$. Finally, $\mathbf{F}_{ij}^{eq}$ can be calculated by substituting Eq. (24) into Eq. (18) and integrating analytically in the velocity space.

Case B: $\Delta t \geqslant 2\tau$, the particle's free transport can be ignored. In this case, the ratio of particles without suffering collision is negative, indicating that the flow field can be regarded as the continuous one, and the distribution function at the cell interface $f(\mathbf{x}_{ij}, t_e)$ can be written as

$$\begin{aligned} f(\mathbf{x}_{ij}, t_e) &= g(\mathbf{x}_{ij}, t_e) - \tau Dg(\mathbf{x}_{ij}, t_e) \\ &\approx g(\mathbf{x}_{ij}, 0) - \tau Dg(\mathbf{x}_{ij}, 0) + t_e \partial_t g(\mathbf{x}_{ij}, 0), \end{aligned} \tag{26}$$

where $Dg(\mathbf{x}_{ij}, 0) = \partial_t g(\mathbf{x}_{ij}, 0) + \boldsymbol{\xi} \cdot \nabla g(\mathbf{x}_{ij}, 0)$ is the substantial derivative of the equilibrium state. Substituting Eq. (26) into Eq. (18), $\mathbf{F}_{ij}^{eq}$ can be determined explicitly, and $\mathbf{F}_i^{fr}$ can be taken as zero. What's more, since Eq. (26) is indeed the expansion of the distribution function truncated to the N-S level, $\mathbf{F}_{ij}^{eq}$ can also be calculated directly by the gas kinetic scheme [41,42] or the N-S solver [43].

B. Calculation of free-streaming fluxes

It can be seen from Sec. III A that the contribution of microscopic particles to the macroscopic fluxes has to be evaluated in the DUGKWP when $\Delta t < 2\tau$. According to Eq. (16), the cumulative distribution for particles' free transport time can be written as

$$\mathcal{G}(t_e) = \frac{2\tau - t_e}{2\tau + t_e}. \tag{27}$$

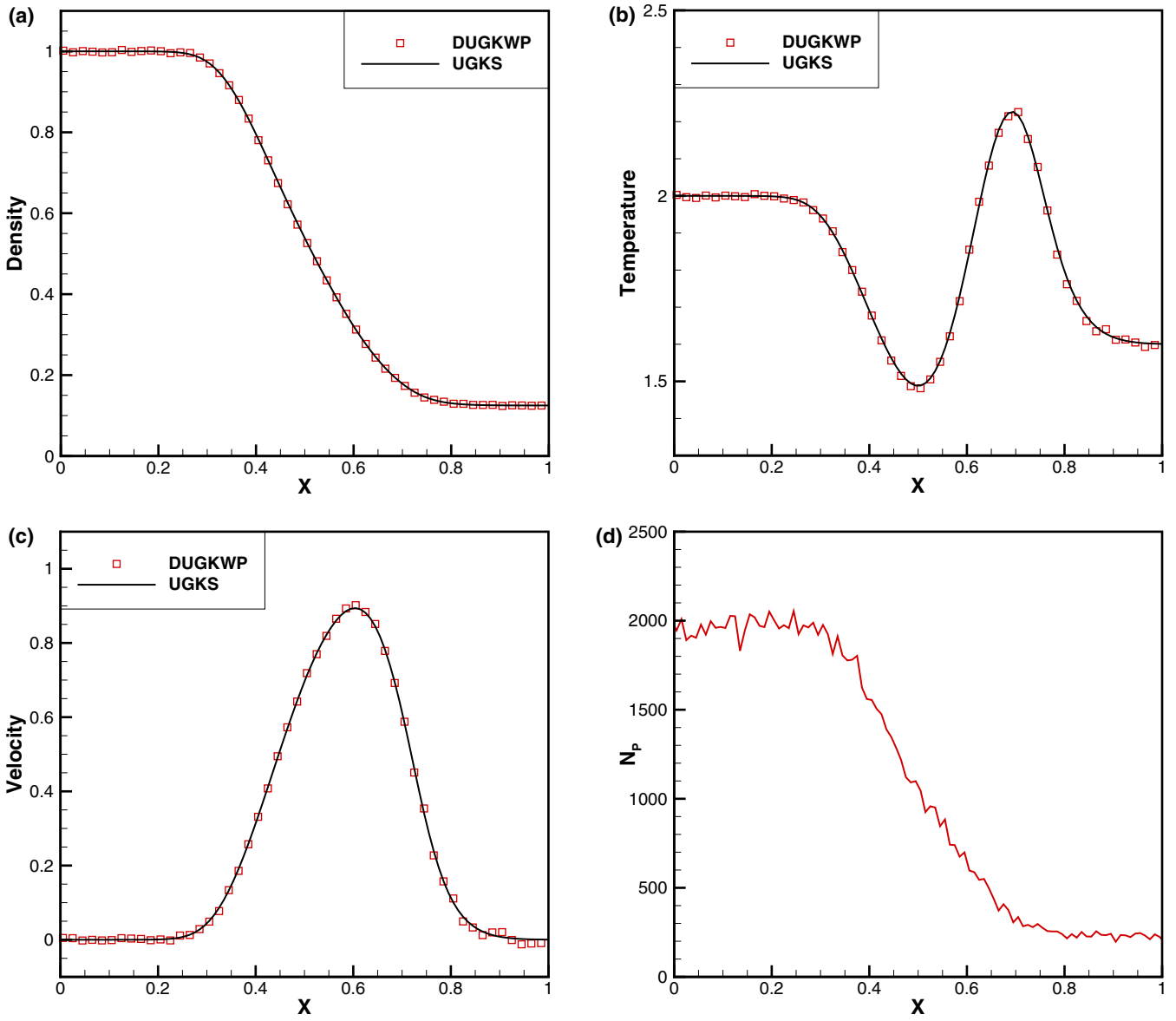

FIG. 5. Distributions of density, temperature, velocity, and number of simulation particles for Sod shock tube problem at $\mu_{\text{ref}} = 10^{-2}$. (a) Density; (b) temperature; (c) velocity; (d) number of simulation particles.

As a result, the free-transport time of a particle within a time step Δt can be evaluated through inversing the above cumulative distribution,

$$t_f = \min\left(\frac{1-r_0}{1+r_0}2\tau, \Delta t\right), \tag{28}$$

where r_0 denotes a random number generated from a uniform distribution between (0, 1). Once the free-transport time is determined, the particle can be accurately tracked by

$$\mathbf{x}_k^{n+1} = \mathbf{x}_k^n + \boldsymbol{\xi}_k t_f. \tag{29}$$

Here the particle velocity $\boldsymbol{\xi}_k$ keeps unchanged during the motion.

According to the free transport time t_f assigned to each particle, we can divide the microscopic particles into the collisionless particle ($t_f = \Delta t$) and the collisional particle ($t_f < \Delta t$). The collisionless particle will not collide with other particles within the time-step size Δt, while at least one collision will occur for the collisional particle. After streaming of all the particles, the free-streaming fluxes of cell i attributed to the particles can be calculated by counting those particles at the beginning and at the end of the time step inside the cell i,

$$\mathbf{F}_i^{fr,p} = \sum_{\mathbf{x}_k^{n+1}\in V_i} \phi_k - \sum_{\mathbf{x}_k^{n}\in V_i} \phi_k, \quad k \in P(i), \tag{30}$$

Where the vector $\phi_k = (m_k, m_k\boldsymbol{\xi}_k, \frac{1}{2}m_k\xi_k^2 + e_k)$ represents the mass, momentum, and energy of the particle k, and $P(i)$ denotes the set of particles inside the cell i. m_k, $\boldsymbol{\xi}_k$, and $e_k = (3-D)R_gT/2$ are the mass, velocity, and potential energy of the particle k, respectively; they can be sampled from the Maxwellian distribution function. Since the contribution of collisional particles to the free-streaming fluxes can be calculated analytically, these particles will be deleted after

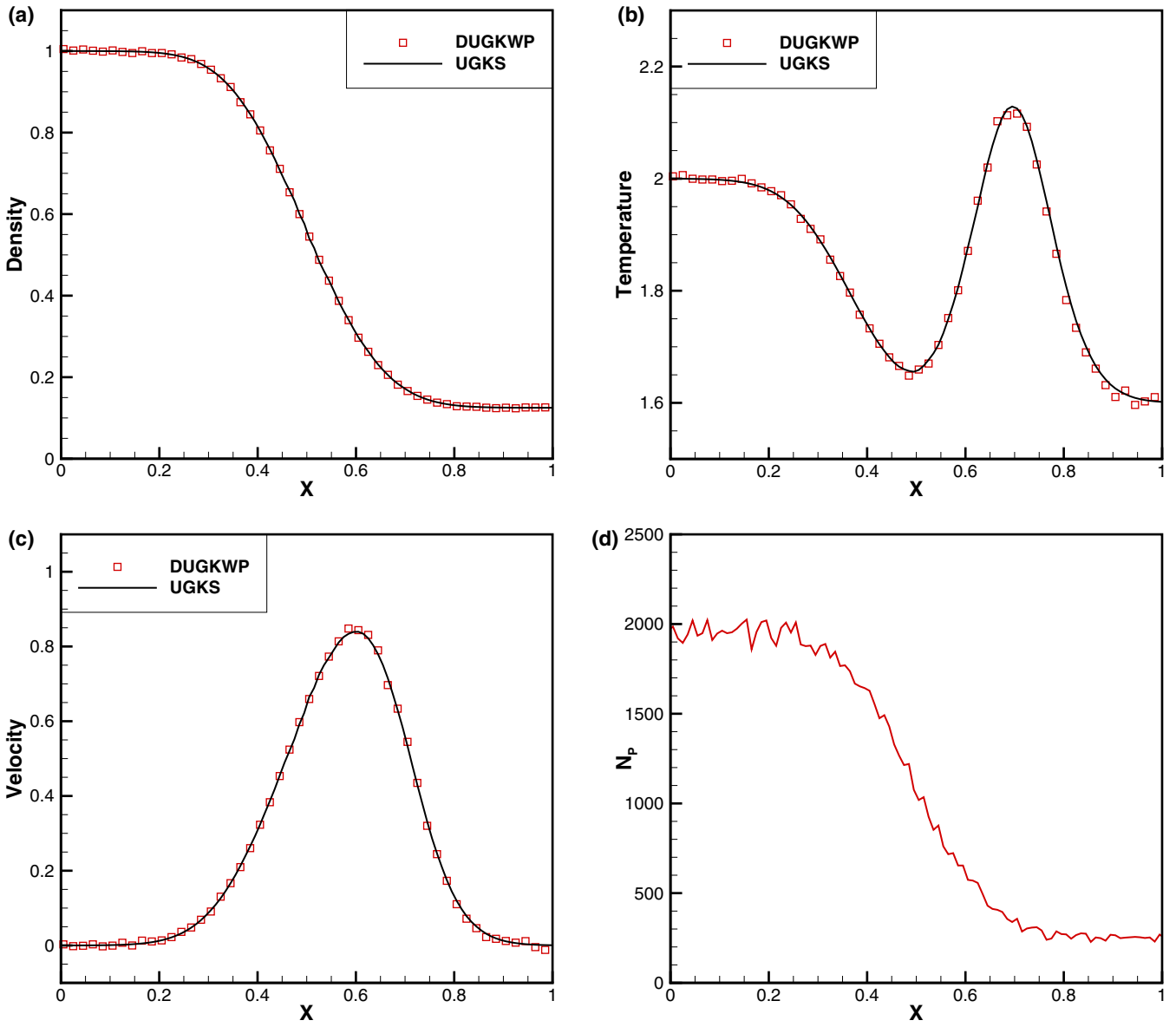

FIG. 6. Distributions of density, temperature, velocity, and number of simulation particles for Sod shock tube problem at $\mu_{\text{ref}} = 10^{-1}$. (a) Density; (b) temperature; (c) velocity; (d) number of simulation particles.

the streaming. Thus, the total conservative flow variables of collisionless part of particles in the cell i after streaming can be calculated by counting those particles at the cell i,

$$\mathbf{W}_i^p = \frac{1}{V_i} \sum_{\mathbf{x}_k^{n+1} \in V_i} \phi_k, \quad k \in P_f(i), \tag{31}$$

where $P_f(i)$ is the set of collisionless particles in the cell i.

According to the conservation, the total conservative flow variables of collisional particles that remained in the cell i after streaming can be calculated by

$$\mathbf{W}_i^h = \mathbf{W}_i^{n+1} - \mathbf{W}_i^p. \tag{32}$$

In fact, $\mathbf{W}_i^h$ and $\mathbf{W}_i^p$ are the macroscopic flow variables corresponding to the hydrodynamic waves and the collisionless particles, respectively. At the beginning of each time step, if we resample particles from $\mathbf{W}_i^h$ directly and classify these particles into the collisionless one and the collisional one, the free-streaming fluxes $\mathbf{F}_i^{fr,p}$ calculated by Eq. (30) are indeed the free-streaming fluxes $\mathbf{F}_i^{fr}$ shown in Eq. (17). This treatment is similar to that of the unified gas-kinetic particle (UGKP) method. Since the total mass of particles in the UGKP equals $\mathbf{W}_i$ consistently in all flow regimes, the computational cost of the UGKP cannot degrade to the N-S solver in the continuum flow regime.

As illustrated in Eqs. (31) and (30), during the free-transport process, the free-streaming fluxes are attributed to both the collisionless particles and the collisional particles, whereas the end of each time step involves only the collisionless particles for the recovery of the nonequilibrium gas distribution function. Thus, we can just resample the collisionless particle at the beginning of each time step and calculate the contribution of collisional particles to the free-streaming fluxes analytically. According to the cumulative distribution Eq. (27), the expectation of the proportion of collisionless

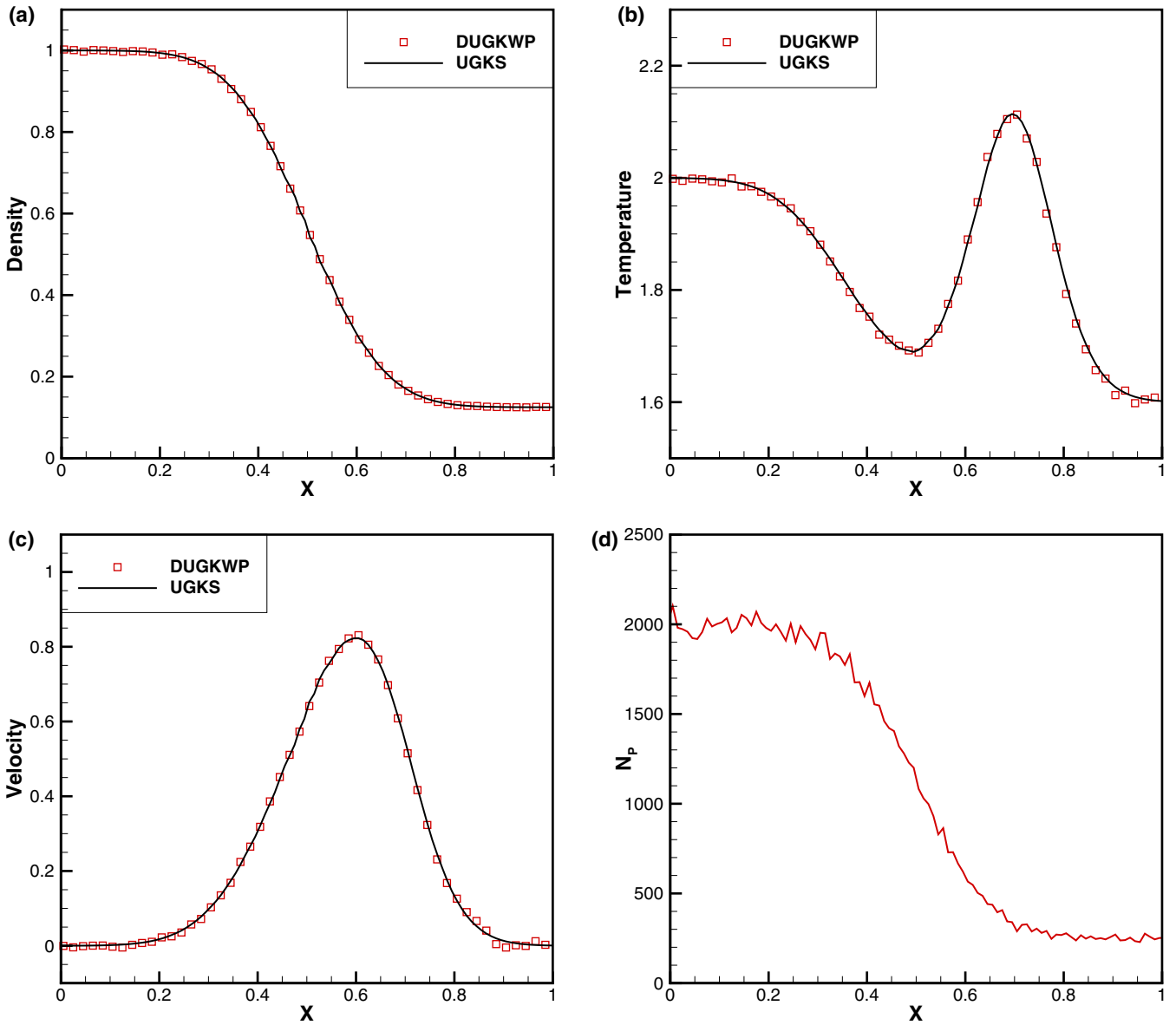

FIG. 7. Distributions of density, temperature, velocity, and number of simulation particles for Sod shock tube problem at $\mu_{\text{ref}} = 10$. (a) Density; (b) temperature; (c) velocity; (d) number of simulation particles.

particles in the cell i can be evaluated at the beginning of each time step from the updated hydrodynamic waves as follows:

$$\mathbf{W}_i^{hp} = \frac{2\tau - \Delta t}{2\tau + \Delta t}\mathbf{W}_i^h = \beta \mathbf{W}_i^h. \tag{33}$$

Equation (33) shows that the proportion of collisionless particles goes to zero as τ approaching $\Delta t/2$, indicating that the number of particles decreases as the weakening of the rarefication effect. Then the macroscopic flow variables corresponding to unsampled particles can be calculated by

$$\mathbf{W}_i^* = \mathbf{W}_i^h - \mathbf{W}_i^{hp}. \tag{34}$$

Similar to the numerical fluxes computed by the stochastic method with free transport mechanics, the contribution of the resampled collisionless particle to the free-streaming fluxes can be calculated by Eq. (30). As for the free-streaming fluxes contributed from $\mathbf{W}_i^*$, it can be calculated analytically by

$$\begin{aligned}
\mathbf{F}_{ij}^{fr,\text{wave}}(\mathbf{W}^*) &= \mathbf{F}_{ij}^{fr,\text{DUGKWP}}(\mathbf{W}^h) - \mathbf{F}_{ij}^{fr,\text{DVM}}(\mathbf{W}^{hp}) \\
&= \frac{1}{\Delta t}\left\langle \boldsymbol{\xi}\boldsymbol{\psi} \int_0^{\Delta t} \frac{2\tau - t_e}{2\tau + t_e} f^h(\mathbf{x}_{ij} - \boldsymbol{\xi} t_e, 0) dt_e \right\rangle \\
&\quad - \frac{1}{\Delta t}\left\langle \boldsymbol{\xi}\boldsymbol{\psi} \int_0^{\Delta t} f^{hp}(\mathbf{x}_{ij} - \boldsymbol{\xi} t_e, 0) dt_e \right\rangle \\
&= \frac{1}{\Delta t}\left\langle \boldsymbol{\xi}\boldsymbol{\psi} \int_0^{\Delta t} \frac{2\tau - t_e}{2\tau + t_e} [g^h(\mathbf{x}_{ij}, 0) \right. \\
&\quad \left. - \tau D g^h(\mathbf{x}_{ij}, 0) - t_e \boldsymbol{\xi} \cdot \nabla g^h(\mathbf{x}_{ij}, 0)] dt_e \right\rangle \\
&\quad - \frac{\beta}{\Delta t}\left\langle \boldsymbol{\xi}\boldsymbol{\psi} \int_0^{\Delta t} [g^h(\mathbf{x}_{ij}, 0) \right.
\end{aligned}$$

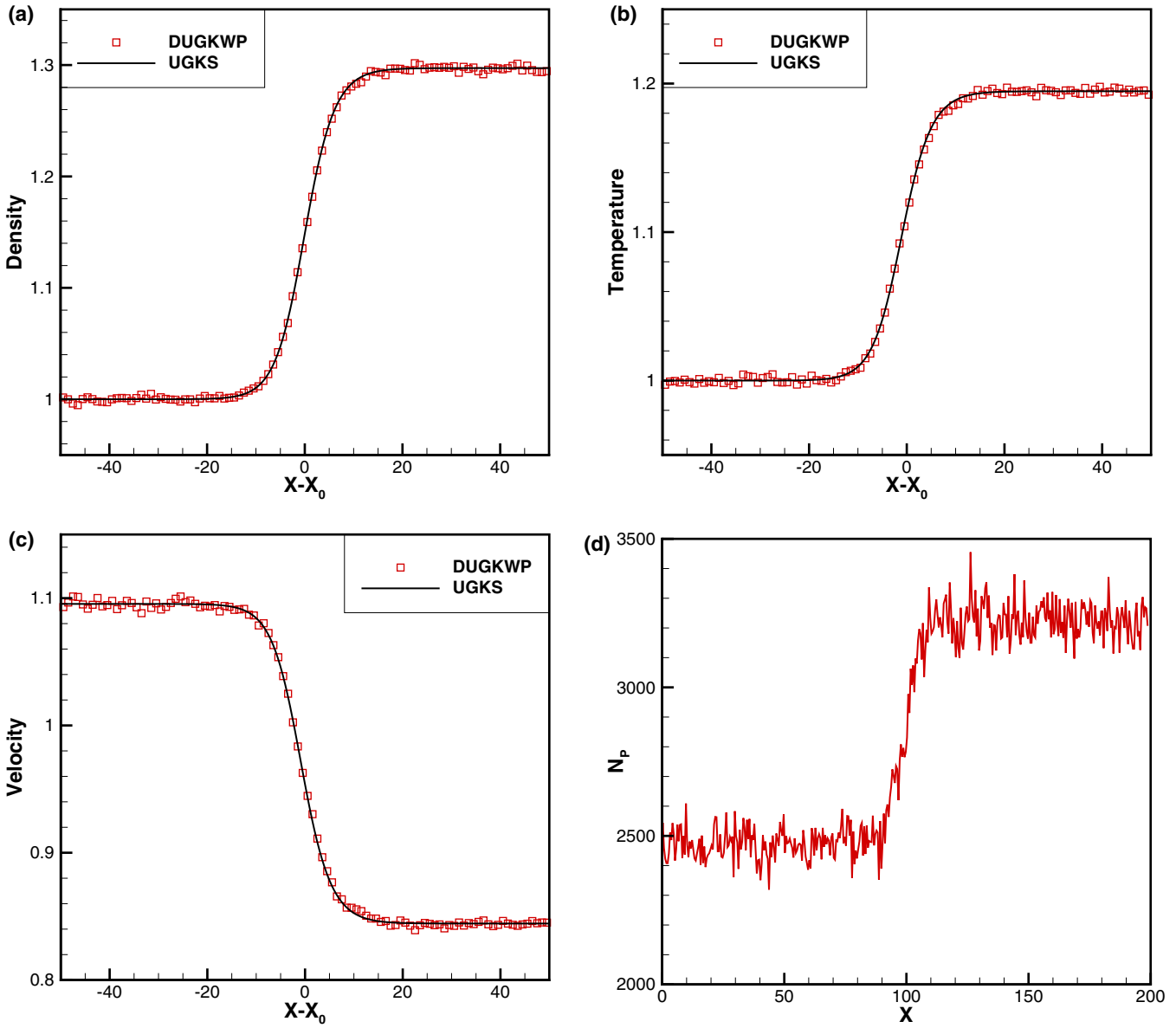

FIG. 8. Distributions of density, temperature, velocity, and number of simulation particles for shock structure at Ma = 1.2. (a) Density; (b) temperature; (c) velocity; (d) number of simulation particles.

$$
\begin{aligned}
&- \tau D g^h(\mathbf{x}_{ij},0) - t_e \boldsymbol{\xi}\cdot\nabla g^h(\mathbf{x}_{ij},0)]dt_e\Big\rangle \\
&= \frac{1}{\Delta t}\langle \boldsymbol{\xi}\boldsymbol{\psi}[c_3 g^h(\mathbf{x}_{ij},0) \\
&\quad + c_4\boldsymbol{\xi}\cdot\nabla g^h(\mathbf{x}_{ij},0) + c_5\partial_t g^h(\mathbf{x}_{ij},0)]\rangle. \quad (35)
\end{aligned}
$$

By using the rectangular rule to approximate the time integration over $[0, \Delta t]$, the coefficients c_3, c_4, and c_5 in Eq. (35) can be written as

$$
\begin{aligned}
c_3 &= \frac{2\tau - h}{2\tau + h}\Delta t - \beta\Delta t, \\
c_4 &= -\frac{2\tau - h}{2\tau + h}(\tau + h)\Delta t + \beta(\tau + h)\Delta t, \\
c_5 &= -\frac{2\tau - h}{2\tau + h}\tau\Delta t + \beta\tau\Delta t. \quad (36)
\end{aligned}
$$

In Eq. (35), g^h is the equilibrium state determined from $\mathbf{W}_i^h$. For better numerical stability, the discontinuity of the equilibrium distribution function and its derivatives at the cell interface can be introduced into Eq. (35), which yields

$$
\begin{aligned}
\mathbf{F}_{ij}^{fr,\text{wave}}(\mathbf{W}^*) &= \frac{c_3}{\Delta t}\langle \boldsymbol{\xi}\boldsymbol{\psi}\{H(\mathbf{n}_{ij}\cdot\boldsymbol{\xi})g^{h,L}(\mathbf{x}_{ij},0) \\
&\quad + [1 - H(\mathbf{n}_{ij}\cdot\boldsymbol{\xi})]g^{h,R}(\mathbf{x}_{ij},0)\}\rangle \\
&\quad + \frac{c_4}{\Delta t}\langle \boldsymbol{\xi}\boldsymbol{\psi}\{H(\mathbf{n}_{ij}\cdot\boldsymbol{\xi})\boldsymbol{\xi}\cdot\nabla g^h(\mathbf{x}_i,0) \\
&\quad + [1 - H(\mathbf{n}_{ij}\cdot\boldsymbol{\xi})]\boldsymbol{\xi}\cdot\nabla g^h(\mathbf{x}_j,0)\}\rangle \\
&\quad + \frac{c_5}{\Delta t}\langle \boldsymbol{\xi}\boldsymbol{\psi}\{H(\mathbf{n}_{ij}\cdot\boldsymbol{\xi})\partial_t g^h(\mathbf{x}_i,0) \\
&\quad + [1 - H(\mathbf{n}_{ij}\cdot\boldsymbol{\xi})]\partial_t g^h(\mathbf{x}_j,0)\}\rangle. \quad (37)
\end{aligned}
$$

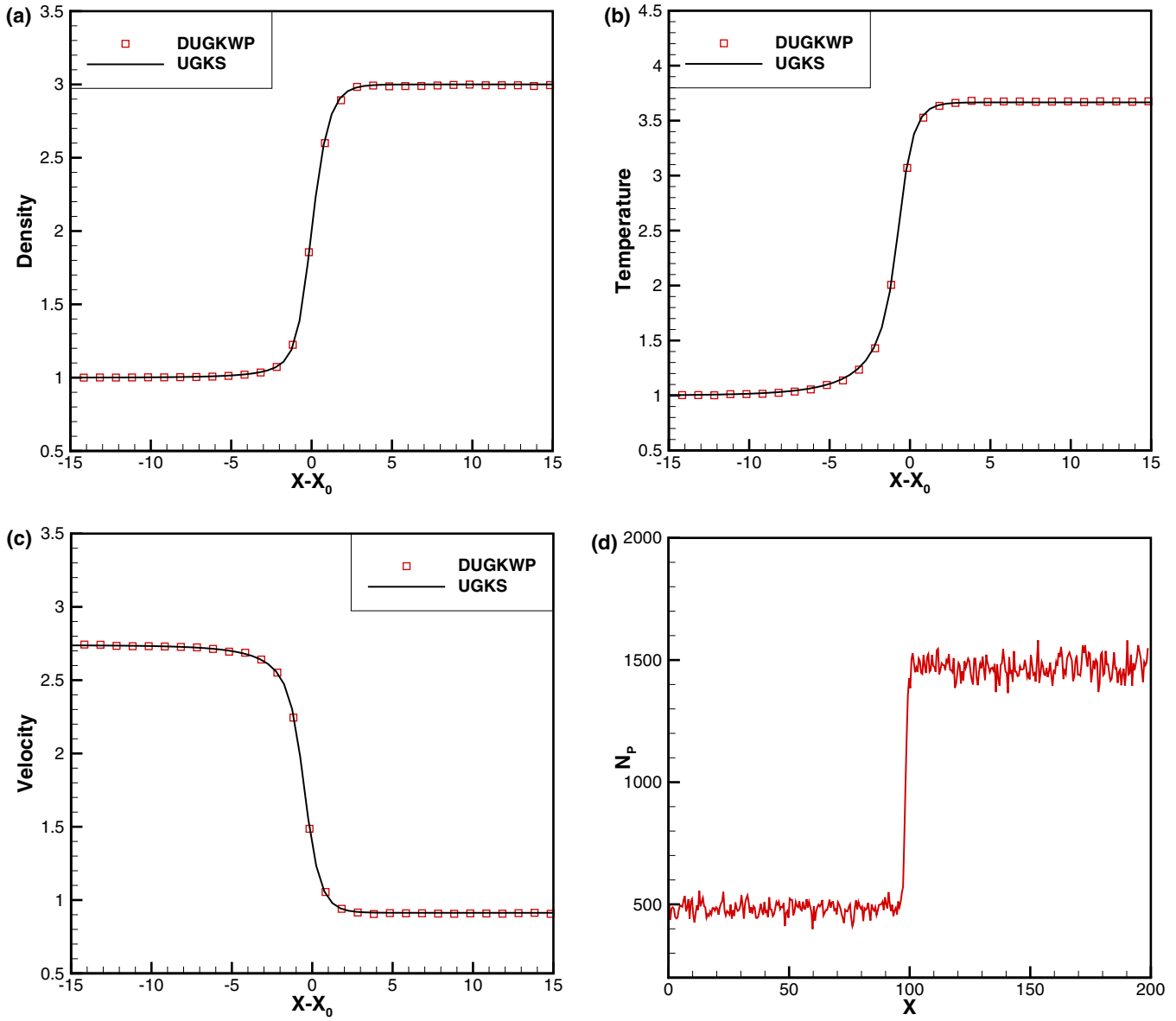

FIG. 9. Distributions of density, temperature, velocity, and number of simulation particles for shock structure at Ma = 3. (a) Density; (b) temperature; (c) velocity; (d) number of simulation particles.

The spatial and temporal derivatives of the equilibrium distribution function at the cell centers of the left and right cells can be calculated by the following micro-macro relationships

$$\nabla \mathbf{W}^h(\mathbf{x}_i, 0) = \langle \boldsymbol{\psi} \nabla g^h(\mathbf{x}_i, 0) \rangle,$$
$$\nabla \mathbf{W}^h(\mathbf{x}_j, 0) = \langle \boldsymbol{\psi} \nabla g^h(\mathbf{x}_j, 0) \rangle, \tag{38}$$

$$\langle \boldsymbol{\psi} \partial_t g^h(\mathbf{x}_i, 0) \rangle = -\langle \boldsymbol{\psi} \boldsymbol{\xi} \cdot \nabla g^h(\mathbf{x}_i, 0) \rangle,$$
$$\langle \boldsymbol{\psi} \partial_t g^h(\mathbf{x}_j, 0) \rangle = -\langle \boldsymbol{\psi} \boldsymbol{\xi} \cdot \nabla g^h(\mathbf{x}_j, 0) \rangle. \tag{39}$$

Finally, the evolution of the conservative flow variables in the DUGKWP can be rewritten as

$$\mathbf{W}_i^{n+1} = \mathbf{W}_i^n - \frac{\Delta t}{V_i} \sum_{j \in N(i)} S_{ij} \mathbf{n}_{ij} \cdot \mathbf{F}_{ij}^{eq} - \frac{\Delta t}{V_i} \sum_{j \in N(i)} S_{ij} \mathbf{n}_{ij} \cdot \mathbf{F}_{ij}^{fr,\text{wave}} + \frac{\mathbf{F}_i^{fr,p}}{V_i}. \tag{40}$$

It can be seen from Eq. (40) that the free-streaming fluxes $\mathbf{F}_i^{fr}$ in Eq. (17) have been divided into two parts in the DUGKWP, $\mathbf{F}_{ij}^{fr,\text{wave}}$ and $\mathbf{F}_i^{fr,p}$. This strategy makes the DUGKWP efficient in the near continuum and continuum flow regimes.

C. Computational sequence

In the DUGKWP, the conservation laws of the conservative flow variables are the key to updating the flow field. For the nonequilibrium flow, both the hydrodynamic waves and the microscopic particles need to be considered since both of them contribute to the calculation of macroscopic fluxes. The interplay of the hydrodynamic waves and the microscopic particles is illustrated in Fig. 1. The summary of computational processes in the DUGKWP is given as follows:

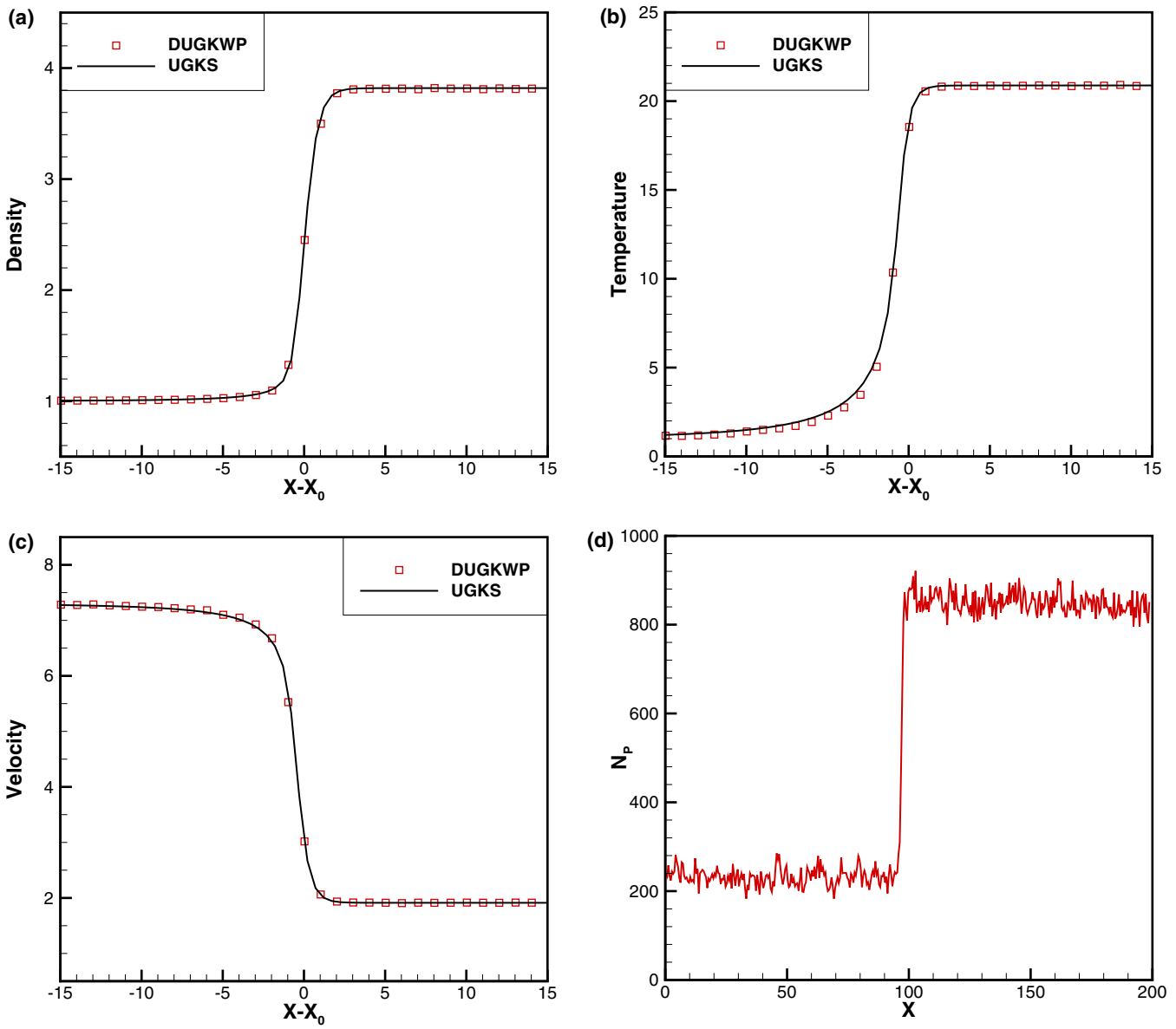

FIG. 10. Distributions of density, temperature, velocity, and number of simulation particles for shock structure at Ma = 8. (a) Density; (b) temperature; (c) velocity; (d) number of simulation particles.

(1) At the beginning of each time step, calculate the ratio of particles without suffering collision $\beta = (2\tau - \Delta t)/(2\tau + \Delta t)$ from $\mathbf{W}_i^n$.

Case A: If $\beta < 0$, the flow field can be regarded as the continuous one. Thus, $\mathbf{F}_{ij}^{eq}$ can be calculated by the N-S solver directly and $\mathbf{F}_i^{fr}$ can be taken as zero. Then the conservative flow variables can be updated by Eq. (17). Go to step (7) for checking the result.

Case B: If $\beta > 0$, the particle's free transport has to be considered. In this situation, $\mathbf{F}_{ij}^{eq}$ can be calculated by Eq. (18), where the time integration of $f_{ij}^{eq}(t_e)$ is determined by Eq. (24).

(2) Get the initial state of particles, which includes the collisionless particles evolved from the previous step $\mathbf{W}_i^{p,n-1}$ and the collisionless particles resampled from the hydrodynamics waves at the current step $\mathbf{W}_i^{hp,n}$, as shown in Fig. 1(b). For the first step, we can take $\mathbf{W}_i^{p,n-1} = \mathbf{0}$ and $\mathbf{W}_i^{hp,n} = \beta \mathbf{W}_i^{h,n} = \beta \mathbf{W}_i^{n=0}$, as shown in Fig. 1(a).

(3) Calculate the free-transport time t_f by Eq. (28) and classify the particles $\mathbf{W}_i^{p,n-1}$ into the collisionless particle (hollow circle) and the collisional particle (filled circle). For the particles resampled from $\mathbf{W}_i^{hp,n}$, their free transport time is always taken as Δt, as shown in Fig. 1(c).

(4) Stream all particles according to Eq. (29) and calculate the free-streaming fluxes $\mathbf{F}_i^{fr,p}$ by Eq. (30). After streaming, delete the collisional particles and update the total conservative flow variables of collisionless particles $\mathbf{W}_i^{p,n}$ by Eq. (31), as shown in Fig. 1(d).

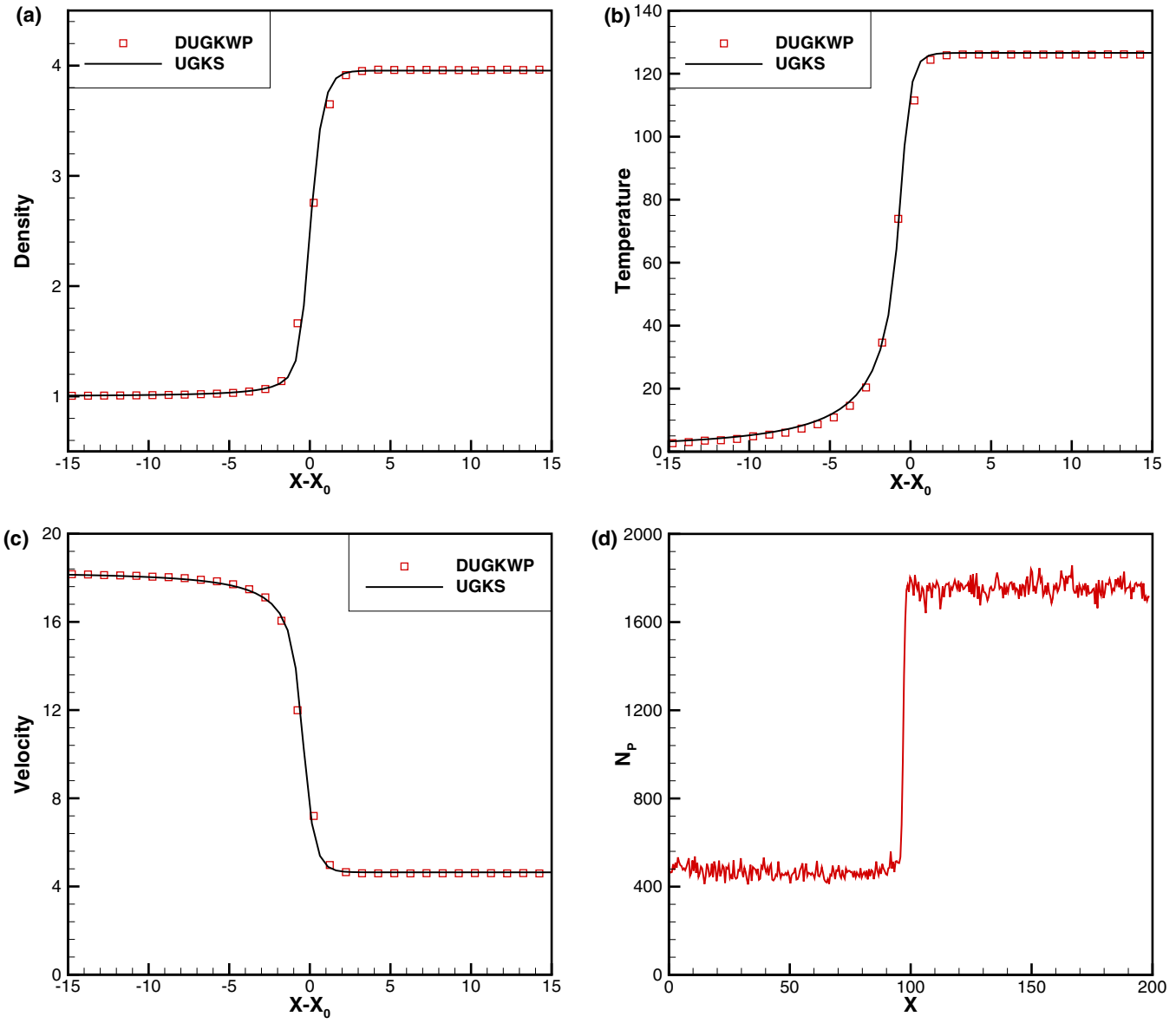

FIG. 11. Distributions of density, temperature, velocity, and number of simulation particles for shock structure at Ma = 20. (a) Density; (b) temperature; (c) velocity; (d) number of simulation particles.

(5) Calculate the free-streaming fluxes $\mathbf{F}_{ij}^{fr,\text{wave}}$ attributed to the hydrodynamic waves of the unsampled particles $\mathbf{W}_i^{h,n} - \mathbf{W}_i^{hp,n}$ by Eq. (37).

(6) Compute the conservative flow variables $\mathbf{W}_i^{n+1}$ through Eq. (40) and the hydrodynamic waves $\mathbf{W}_i^{h,n+1}$ through Eq. (32). Calculate the proportion of collisionless particles for the next time step $\mathbf{W}_i^{hp,n+1}$ by Eq. (33) if $\beta > 0$.

(7) Repeat steps (1) to (6) until the convergence result is obtained.

D. Analysis and discussion

As a numerical method for simulation of multiscale fluid flow problems, the asymptotic behaviors of the DUGKWP in the collisionless limit and the continuous limit are analyzed in this section.

(1) Collisionless limit ($\tau \to \infty$). In this case, the collision time τ is far larger than the time-step size Δt. Thus, we have

$$\beta = \lim_{\tau\to\infty} (2\tau - \Delta t)/(2\tau + \Delta t) \to 1,$$
$$t_f = \lim_{\tau\to\infty} \left\{ \min\left(\frac{1 - r_0}{1 + r_0} 2\tau, \Delta t \right) \right\} \to \Delta t. \tag{41}$$

Equation (41) shows that the ratio of particles without suffering collision approaches one, and all these particles will be streamed with time step Δt, indicating that the DUGKWP solves the collisionless Boltzmann equation in this situation.

(2) Continuous limit ($\tau \to 0$). As a multiscale approach, the time-step size of the DUGKWP is not constrained by the collision time τ. Thus, the collision time τ will be far less than the time-step size Δt in the continuous limit. If $\tau < \Delta t/2$, the ratio of particles without suffering collision becomes negative and the macroscopic fluxes are fully determined by the N-S

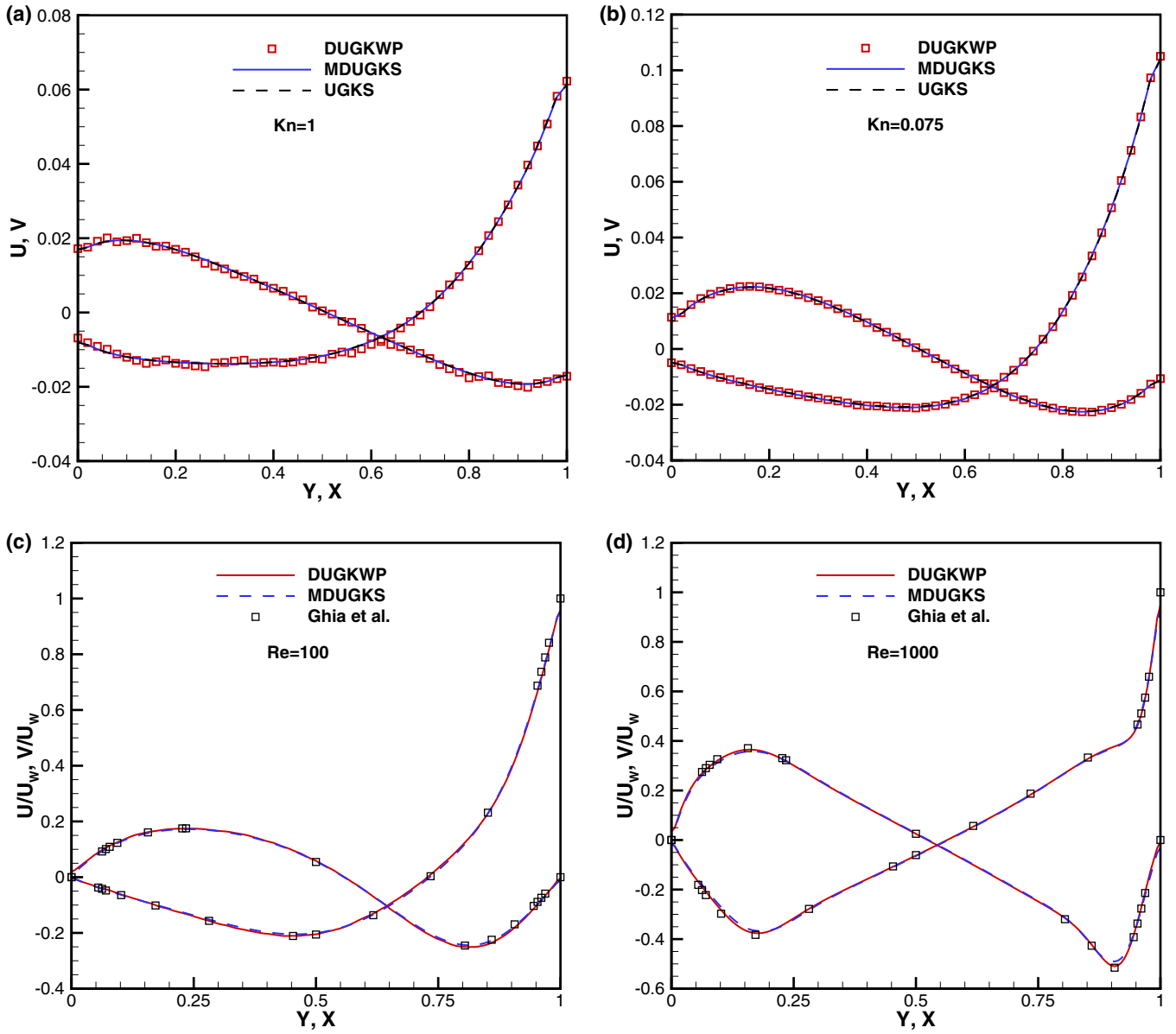

FIG. 12. Comparison of velocity profiles along the vertical and horizontal central lines for lid-driven cavity flow at different Reynolds and Knudsen numbers. (a) Kn = 1; (b) Kn = 0.075; (c) Re = 100; (d) Re = 1000.

solver. Consequently, the solution given by the DUGKWP in this situation is indeed the result of the N-S equations.

In the critical state of $\tau = \Delta t/2$, the collisionless particle vanishes and $\mathbf{W}^h = \mathbf{W}$. According to Eqs. (24) and (37) without considering the discontinuity of equilibrium distribution functions and their derivatives, the macroscopic fluxes at the cell interface can be written as

$$\begin{aligned}\mathbf{F}_{ij}^{eq} + \mathbf{F}_{ij}^{fr,\text{wave}} &= \frac{1}{\Delta t}\{\langle \boldsymbol{\xi}\boldsymbol{\psi}(2c_1 g - c_2 \boldsymbol{\xi}\cdot\nabla g + c_2\partial_t g)\rangle \\ &\quad + \langle \boldsymbol{\xi}\boldsymbol{\psi}(c_3 g + c_4 \boldsymbol{\xi}\cdot\nabla g + c_5\partial_t g)\rangle\} \\ &= \left\langle \boldsymbol{\xi}\boldsymbol{\psi}\left[g(\mathbf{x}_{ij},0) - \tau D g(\mathbf{x}_{ij},0) \right.\right. \\ &\quad \left.\left. + \frac{\Delta t}{2}\partial_t g(\mathbf{x}_{ij},0)\right]\right\rangle. \end{aligned} \tag{42}$$

Equation (42) shows that the macroscopic fluxes in the critical state are actually the N-S fluxes given by the first-order Chapman-Enskog expansion. It is confirmed that the DUGKWP will reduce to the N-S solver at $\tau = \Delta t/2$.

IV. NUMERICAL EXAMPLES

In this section a series of test cases, including the Sod shock tube, the shock structure, the lid-driven cavity flow, and the hypersonic flow around a circular cylinder, are simulated to assess the performance of the DUGKWP. The results of the DUGKWP will be compared with those of the UGKS and/or the modified DUGKS (MDUGKS) shown in Sec. II. For simplicity, the monatomic gas is assumed in all simulations, where the specific heat ratio is taken as 5/3, the Prandtl number is set as 1, and the gas constant is chosen as 208.13. In addition, all computations are carried out on a PC with an

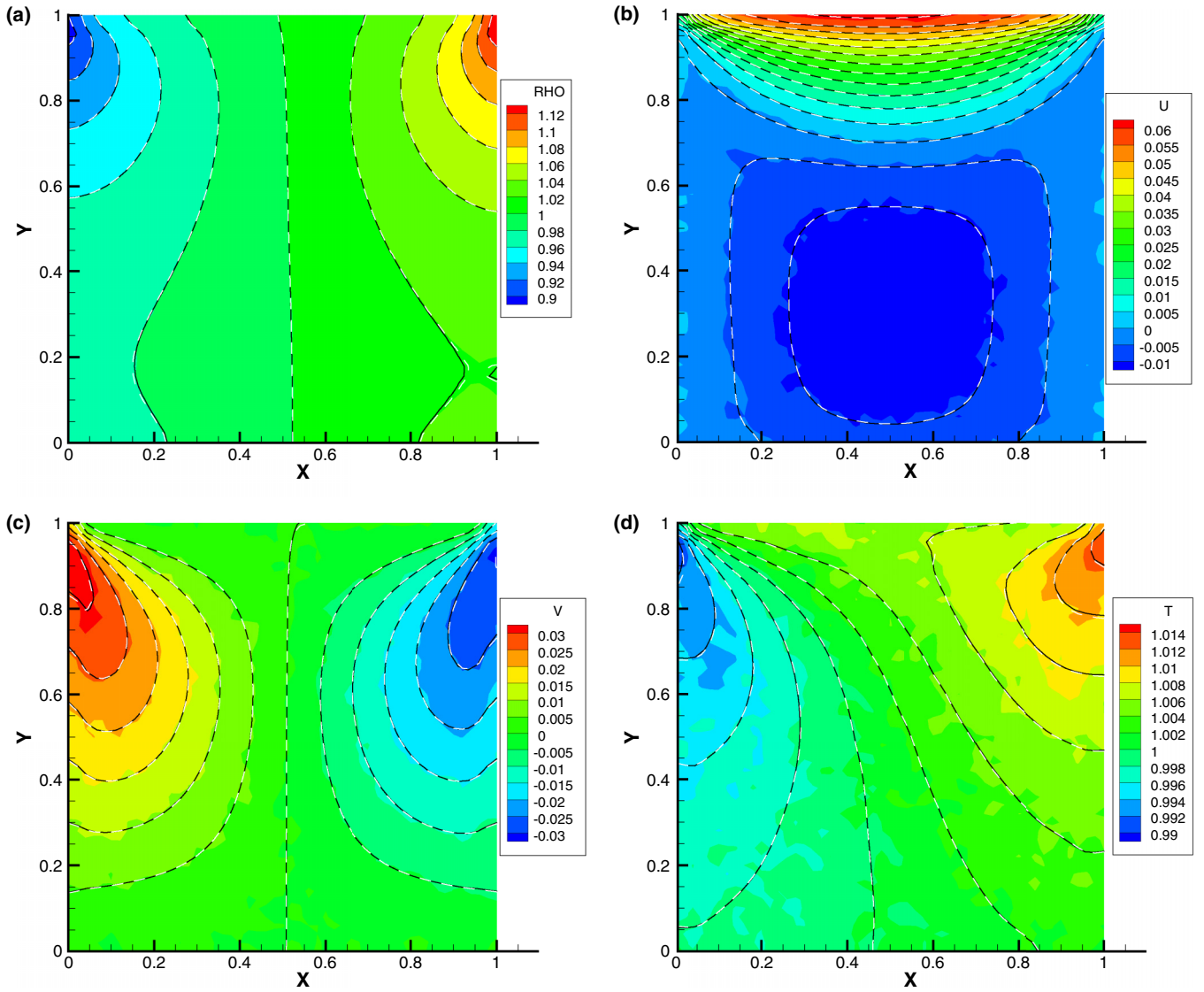

FIG. 13. Comparison of density, u velocity, v velocity, and temperature contours for lid-driven cavity flow at Kn = 1 (DUGKWP: colored background; MDUGKS: white dash line; UGKS: black solid line). (a) Density; (b) u velocity; (c) v velocity; (d) temperature.

Intel® Xeon® Gold 6226R CPU @2.9 GHz processor. For the simplicity of comparing efficiency, we decided not to use parallelization.

A. Case 1: Sod shock tube

The first test case is the Sod shock tube problem with different Knudsen numbers. In the simulations, the computational domain of [0,1] is divided uniformly into 100 cells, and the initial condition is taken as

$$(\rho_1, u_1, p_1) = (1, 0, 1), \quad 0 < x < 0.5$$
$$(\rho_2, u_2, p_2) = (0.125, 0, 0.1), \quad 0.5 \leqslant x < 1 \tag{43}$$

The dynamic viscosity is calculated by

$$\mu = \mu_{\text{ref}} \left(\frac{T}{T_{\text{ref}}} \right)^{w}, \tag{44}$$

where T_{ref} and μ_{ref} are the reference temperature and reference dynamic viscosity, respectively. w is a constant related to the intermolecular interaction models. In this work, the hard sphere (HS) model with $w = 0.5$ is adopted for all simulations by the DUGKWP, UGKS, and MDUGKS. As the Knudsen number is proportional to the reference dynamic viscosity, different values of μ_{ref} will be simulated to evaluate the performance of the DUGKWP in different flow regimes.

In this test case, the reference dynamic viscosity μ_{ref} is varied from $\mu_{\text{ref}} = 10^{-5}$ to $\mu_{\text{ref}} = 10$, resulting in the corresponding Knudsen number defined by the left initial state changes from $\text{Kn} = \frac{16}{5\sqrt{\pi}}\mu_{\text{ref}} = 1.805 \times 10^{-5}$ to 18.05, which covers the flow regimes from the continuum to the free molecular one. The simulation results of the present method will be compared with the UGKS [27]. When using the UGKS, the dimensionless molecular velocity space truncated to $[-15, 15]$, which covers all possible distribution functions in the whole physical space, is discretized uniformly by 201 points and the Newton-Cotes quadrature is utilized for numerical integration. The CFL number is set as 0.95 to guarantee the computational stability, which results in a time-step size of 5×10^{-4}. When

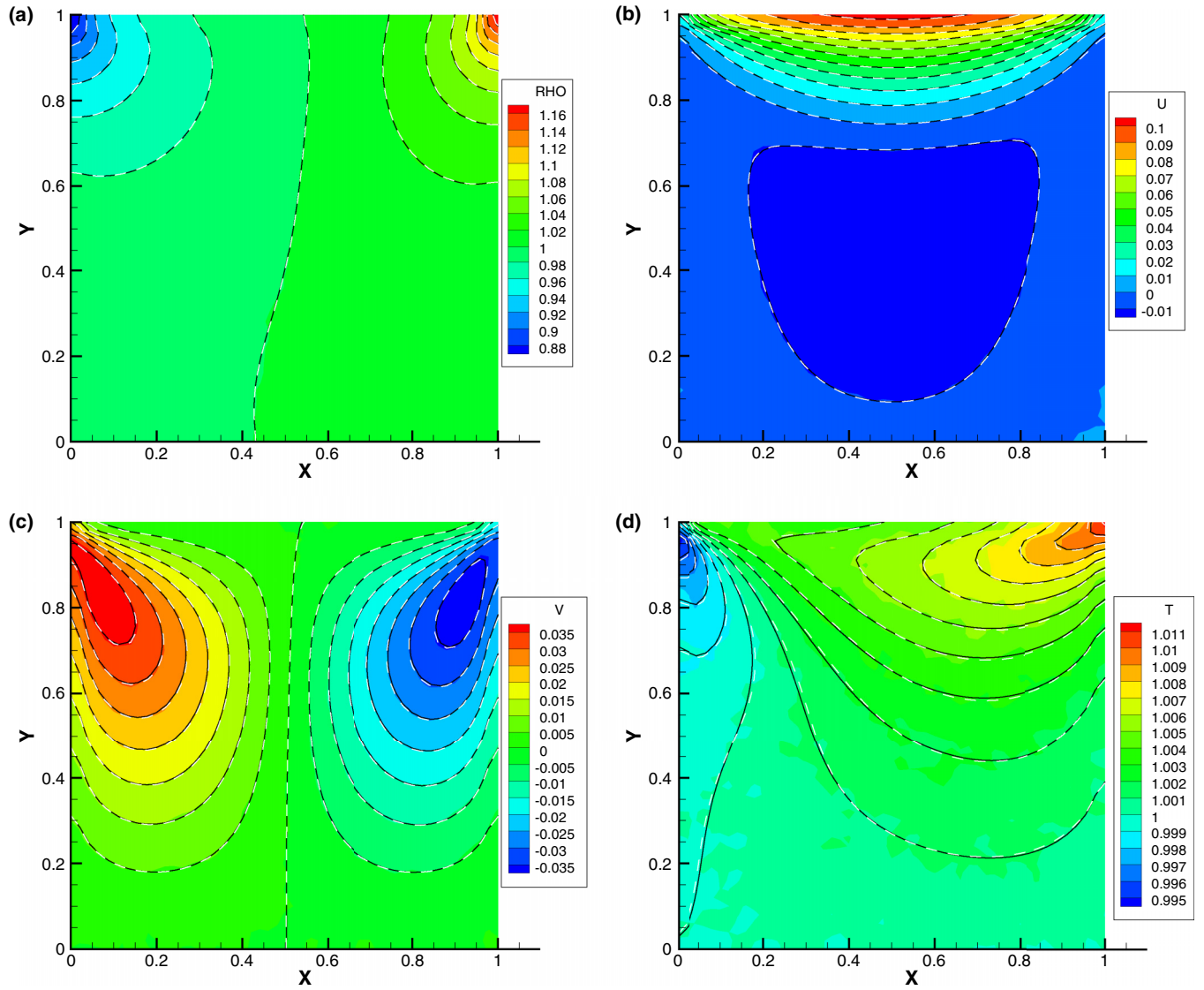

FIG. 14. Comparison of density, u velocity, v velocity, and temperature contours for lid-driven cavity flow at Kn = 0.075 (DUGKWP: colored background; MDUGKS: white dash line; UGKS: black solid line). (a) Density; (b) u velocity; (c) v velocity; (d) temperature.

using the DUGKWP, the mass of the simulation particle is taken as $m_p = 5 \times 10^{-6}$, the time-step size is set the same as that of the UGKS, and 100 separate simulations are used to obtain the averaged solutions.

Figures 2–7 show the distributions of the density, temperature, velocity, and number of simulation particles at $\mu_{\text{ref}} = 10^{-5}$, 10^{-4}, 10^{-3}, 10^{-2}, 10^{-1}, and 10, respectively. The averaged solutions calculated by the DUGKWP method correspond well with the results of the UGKS, which validates the effectiveness of the present method in all flow regimes. In addition, it can be noticed from the distribution of the number of simulation particles that the number of simulation particles approaches zero in the continuum flow regime and increases gradually as the increasing of reference dynamic viscosity μ_{ref}, namely, the enhancing of the rarefaction effect. This observation indicates that the computational cost of the DUGKWP method can be reduced to the N-S solver in the continuum flow regime.

B. Case 2: Shock structure

The second test case is the shock structure with different Mach numbers of 1.2, 3, 8, and 20. In the simulation, the computational domain of $x \in [-50\lambda_{\text{ref}}, 50\lambda_{\text{ref}}]$ is divided uniformly into 200 cells, where λ_{ref} is the mean-free path at the upstream condition. The initial condition is given by the Rankine-Hugoniot condition. The reference dynamic viscosity is calculated by

$$\mu_{\text{ref}} = \frac{5\sqrt{\pi}}{16}\text{Kn}. \tag{45}$$

In the simulation, the Knudsen number is taken as Kn = 1. Like the first test case, the simulation results of the present method for this test case will also be compared with the UGKS [27]. When using the UGKS to solve the cases of Ma = 1.2, 3, and 8, the molecular velocity space truncated to $[-15, 15]$ is discretized uniformly by 201 points, and the Newton-Cotes quadrature is utilized for numerical integration. For the case of

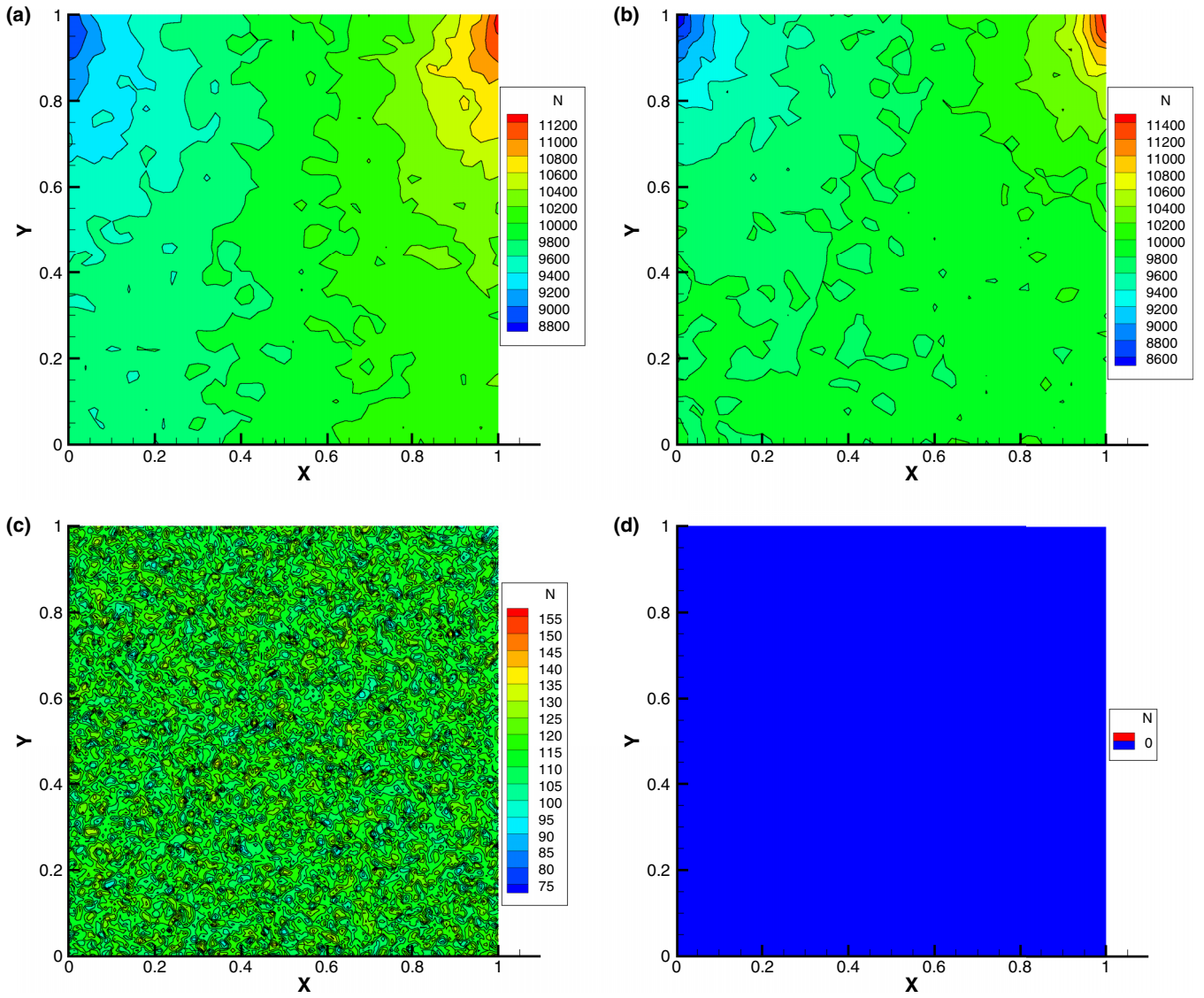

FIG. 15. Distribution of simulation particles for lid-driven cavity flow at different Reynolds/Knudsen numbers. (a) Kn = 1; (b) Kn = 0.075; (c) Re = 100; (d) Re = 1000.

Ma = 20, the truncation region is enlarged to $[-30, 30]$ and the number of discretization points in the molecular velocity space is set as 401. The CFL number is set as 0.95, which results in the time-step size about 2.5×10^{-2} for the cases of Ma = 1.2, 3, and 8 and 1.25×10^{-2} for the case of Ma = 20. When using the DUGKWP, the mass of the simulation particle is taken as $m_p = 2 \times 10^{-4}$, 1×10^{-3}, 2×10^{-3}, and 5×10^{-3} for the cases of Ma = 1.2, 3, 8, and 20, respectively. The time-step size of the DUGKWP method is set the same as that of UGKS, and the last 2000 iterations are used to obtain the averaged solutions.

The distributions of the density, temperature, velocity, and number of simulation particles for shock structure at Ma = 1.2, 3, 8, and 20 are depicted in Figs. 8–11, respectively. Basically, the present results agree well with those of the UGKS. In addition, it can be seen that the thickness of the shock wave at Mach number of 1.2 is larger than those of 3, 8, and 20. Thus, the stronger rarefied gas effect emerges in the case of Ma = 1.2 as compared with those of Ma = 3, 8, and 20. To resolve the shock structure at Mach number of 1.2, more simulation particles are required.

C. Case 3: Lid-driven cavity flow

As a classic benchmark case for assessing the performance of a newly developed method in different flow regimes, the lid-driven cavity flow is studied. In this test case, the top boundary of the cavity moves with a velocity of $u_W = 0.15\sqrt{2R_gT_{\rm ref}}$, where $T_{\rm ref}$ is the wall temperature as well as the reference temperature, and the other boundaries are stationary. Four test cases at different Reynolds and Knudsen numbers; namely, Kn = 1, Kn = 0.075, Re = 100, and Re = 1000, are considered here. For the cases of Kn = 1 and Kn = 0.075, the dynamic viscosity μ is determined by Eq. (44), and the reference dynamic viscosity $\mu_{\rm ref}$ is calculated by

$$\frac{\mu_{\rm ref}}{L} = \frac{5\rho_{\rm ref}(2\pi R_gT_{\rm ref})^{1/2}}{16}{\rm Kn}, \tag{46}$$

TABLE I. Comparison of computational time (hr) and memory cost (MB) of different methods for lid-driven cavity flow at different Reynolds and Knudsen numbers.

	Scheme	Kn = 1	Kn = 0.075	Re = 100	Re = 1000
Computational time	MDUGKS	0.82	0.17	2.71	7.69
	DUGKWP	9.02	8.75	4.05	0.64
	Time ratio	0.09	0.02	0.67	12.02
Memory cost	MDUGKS	2775	333	255	255
	DUGKWP	1909	1909	216	18
	Memory ratio	1.45	0.17	1.18	14.17

Note: All simulations were carried out using an in-house FORTRAN code on a PC with an Intel® Xeon® Gold 6226R CPU at 2.9 GHz processor without the parallelization.

where ρ_{ref} is the reference density and L is the edge length of the cavity. For the cases of Re = 100 and Re = 1000, μ is given by

$$\mu = \frac{\rho_{\text{ref}} u_W L}{\text{Re}}. \tag{47}$$

In the simulation, the computational domain is discretized uniformly by 50 × 50 cells for the first two test cases and by 150 × 150 cells for the last two test cases.

In this test example, we will compare the results of the developed method with those of the UGKS, the MDUGKS,

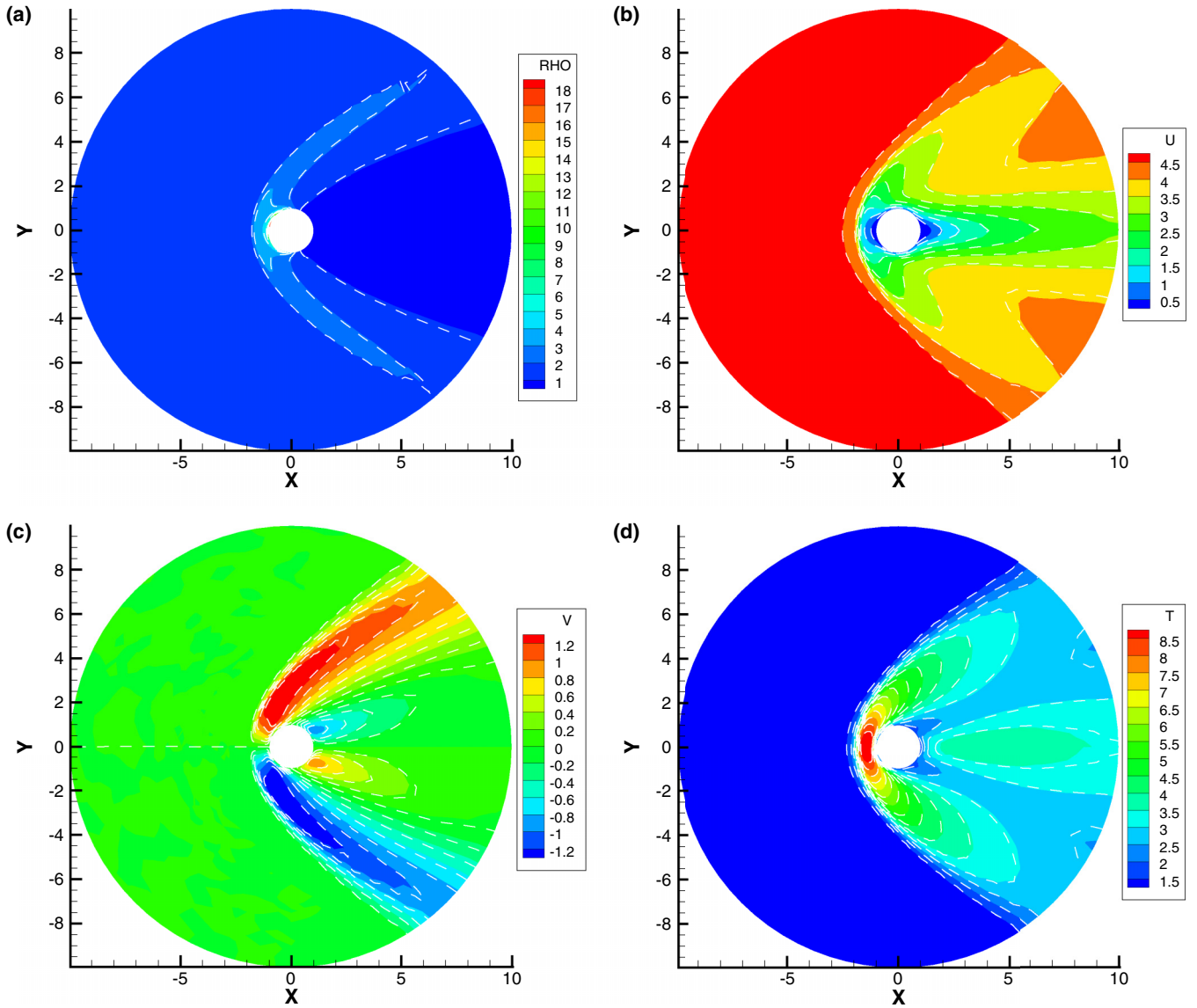

FIG. 16. Comparison of density, u velocity, v velocity, and temperature contours for flow around a circular cylinder at Ma = 5 and Kn = 0.1 (DUGKWP: colored background; MDUGKS: white dash line). (a) Density; (b) u velocity; (c) v velocity; (d) temperature.

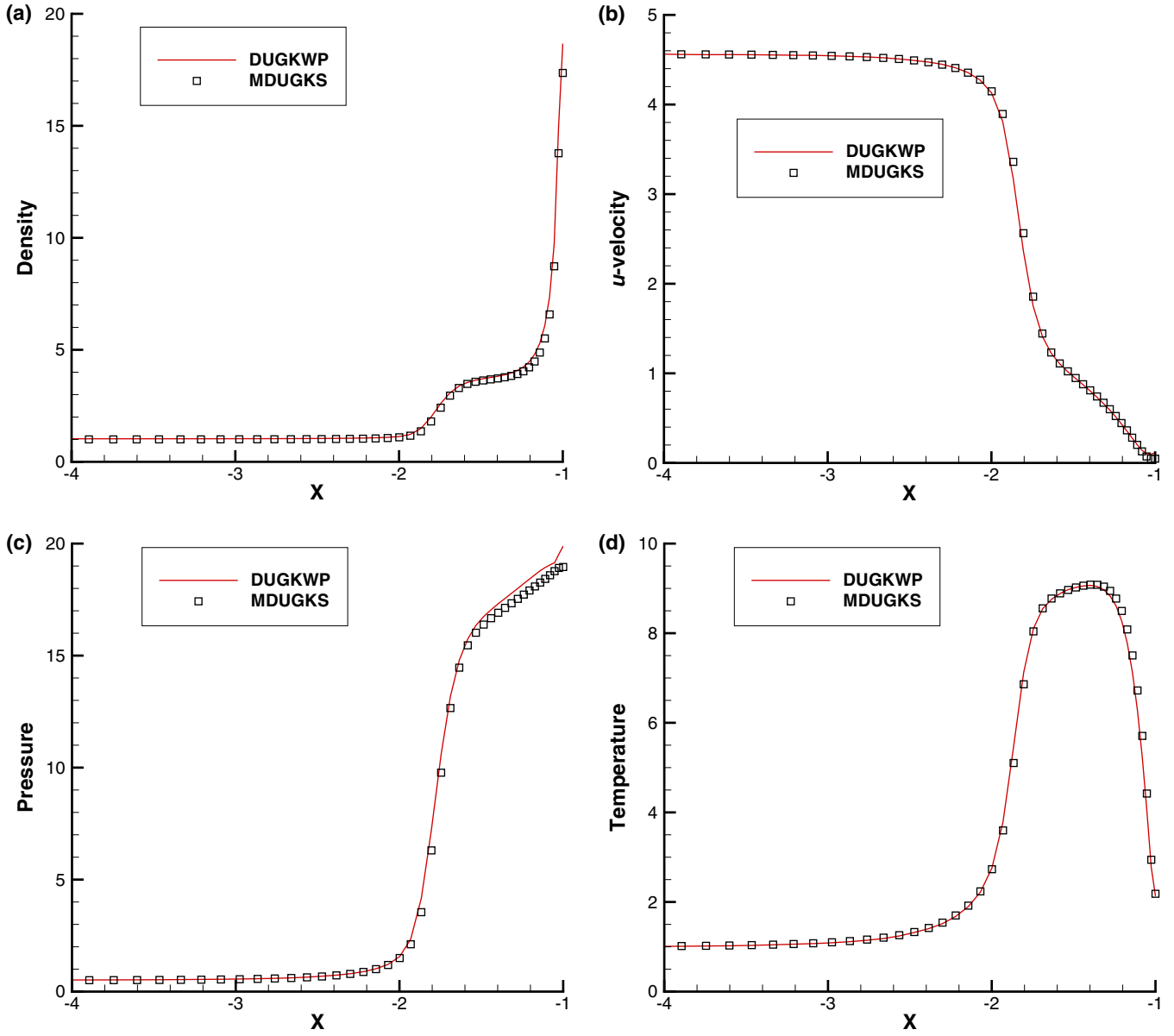

FIG. 17. Comparison of density, u velocity, pressure, and temperature profiles along the stagnation line for flow around a circular cylinder at Ma = 5 and Kn = 0.1. (a) Density; (b) u velocity; (c) pressure; (d) temperature.

and the N-S solver. When using the UGKS and MDUGKS, the Newton-Cotes quadrature with 81×81 points uniformly distributed in $[-4, 4] \times [-4, 4]$ is utilized for the test case of Kn = 1, the Gauss-Hermite quadrature rule with 28×28 points is used for the test case of Kn = 0.075, and the Gauss-Hermite quadrature rule with 8×8 points is used for the last two test cases. The CFL number is set as 0.95. When using the DUGKWP, the mass of the simulation particle is taken as $m_p = 1/(50 \times 50 \times 10000)$ for the first two test cases and $m_p = 1/(150 \times 150 \times 400)$ for the last two test cases, and the time-step size is set the same as that of the UGKS and MDUGKS. The averaged solutions of the last 20 000 iterations are output for comparison.

The velocity profiles along the vertical and horizontal central lines at different Reynolds and Knudsen numbers are compared in Fig. 12. Basically, the results obtained by the DUGKWP agree well with those calculated by using the UGKS and MDUGKS or by Ghia *et al.* [44] using the N-S solver, validating the accuracy of the present method for simulation of low-speed flows in both the rarefied and continuous flow regimes. However, compared with the test case of Kn = 0.075, the results at Kn = 1 calculated by the DUGKWP involve some statistical noise due to the stronger rarefied gas effect. This statistical noise can be reduced by using more simulation particles and statistical sampling times [45]. Figures 13 and 14 compare the density, u velocity, v velocity, and temperature for the cases at Kn = 1 and 0.075 computed by different methods, respectively. The results of the DUGKWP are in general consistent with those of the UGKS and MDUGKS except for the temperature distribution. The reason could be that the temperature is calculated by the higher order of moment of the distribution function as compared with the density and velocity.

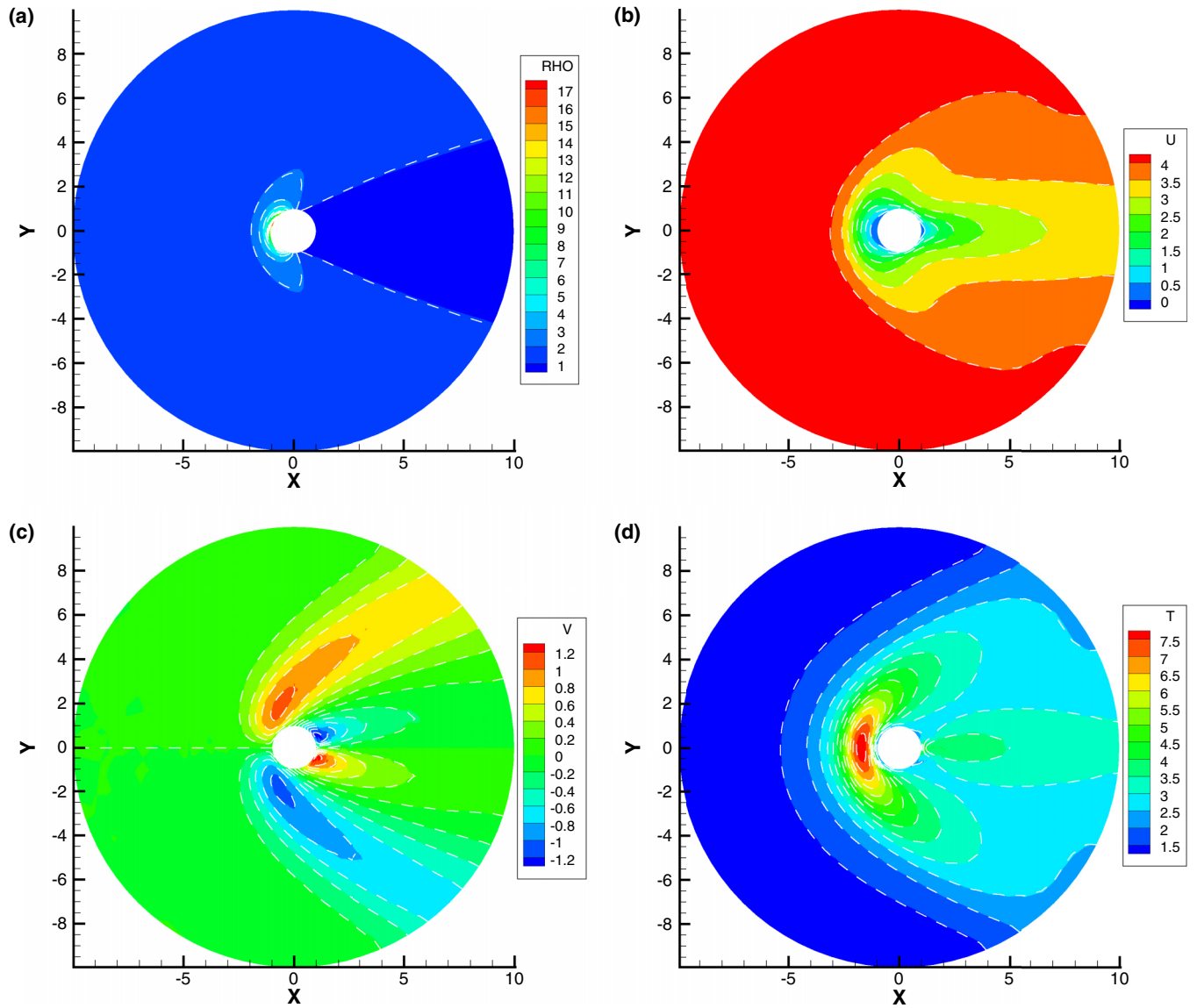

FIG. 18. Comparison of density, u velocity, v velocity, and temperature contours for flow around a circular cylinder at Ma = 5 and Kn = 1 (DUGKWP: colored background; MDUGKS: white dash line). (a) Density; (b) u velocity; (c) v velocity; (d) temperature.

The efficiency and memory consumption of the DUGKWP and MDUGKS are related to the number of simulation particles and discrete velocities, respectively. Figure 15 displays the distribution of simulation particles for the lid-driven cavity flow at different Reynolds and Knudsen numbers. Clearly, the number of simulation particles reduces gradually with the flow transitioning to the continuum flow. For the case of Re = 1000, there is no simulation particle in the computational domain, which means that the DUGKWP reduces to the N-S solver in this circumstance. But for the test cases of Kn = 1 and 0.075, the number of simulation particles in each cell is larger than the number of discrete velocities used for the UGKS and MDUGKS. Correspondingly, the DUGKWP is more efficient and has less memory consumption than the UGKS and MDUGKS for the test case of Re = 1000, while it is inefficient and has relatively high memory consumption as the increasing of the Knudsen number for the simulation of low-speed flows due to the requirement of a large number of particles to reduce the statistical noise, as reported in Table I.

D. Case 4: Flow around a circular cylinder

The last test example is the hypersonic flow around a circular cylinder with different Knudsen numbers of 0.1 and 1, which is used to validate the present method for high-speed flows. In the simulation, the free-stream Mach number is taken as Ma = 5, and the wall temperature is fixed at the free-stream temperature. The reference dynamics viscosity is determined by Eq. (46), in which L is chosen as the radius of the cylinder. A nonuniform mesh with 65 and 80 points in the radial direction and circumferential direction, respectively, is used to discretize the computational domain where a far-field boundary is located at $15L$ away from the geometrical center. When using the MDUGKS, the Newton-Cotes quadrature with 101×101 points uniformly distributed in

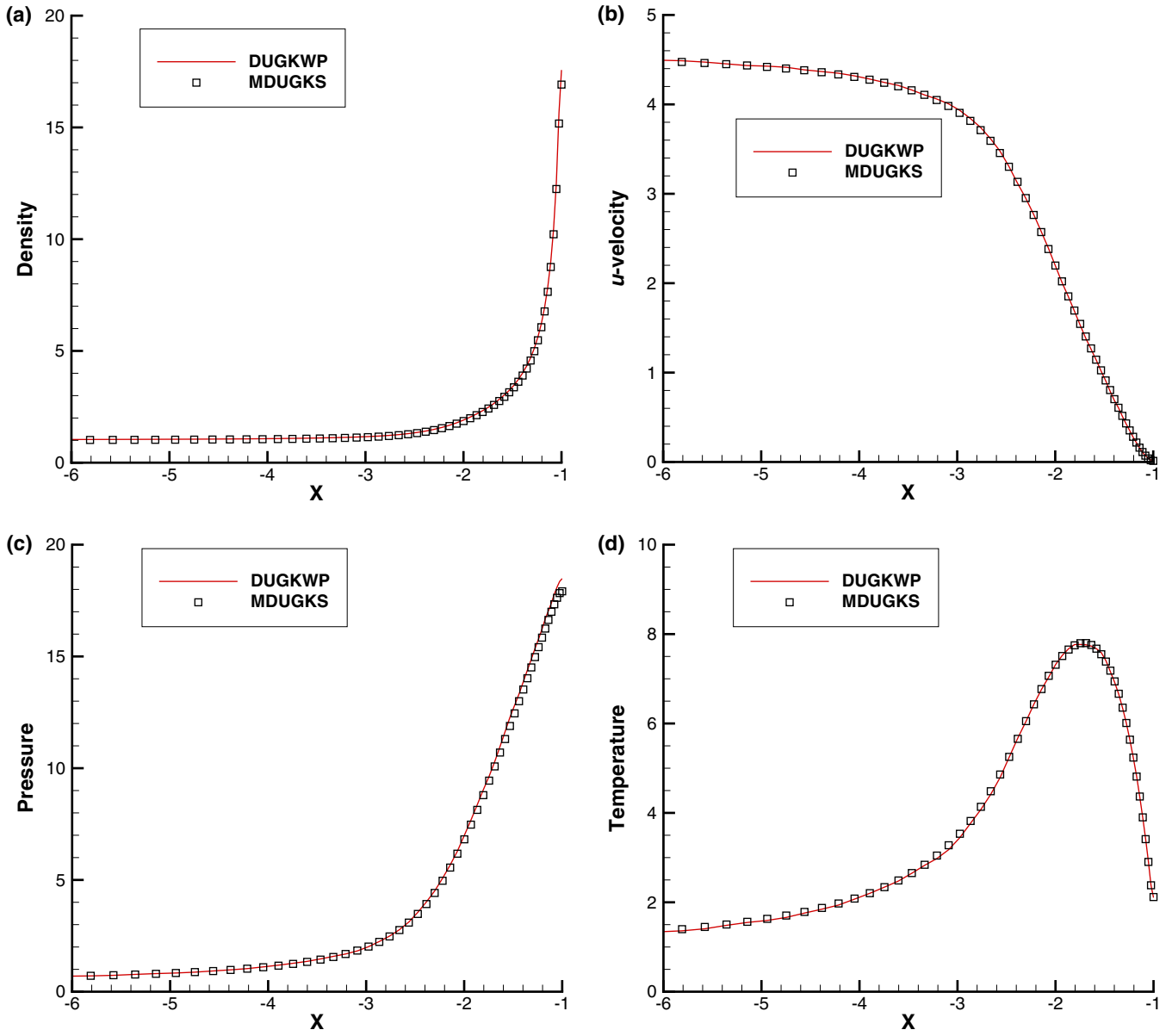

FIG. 19. Comparison of density, u velocity, pressure, and temperature profiles along the stagnation line for flow around a circular cylinder at Ma = 5 and Kn = 1. (a) Density; (b) u velocity; (c) pressure; (d) temperature.

$[-12, 12] \times [-12, 12]$ is utilized for numerical quadrature in the velocity space. When using the DUGKWP, the minimum number of simulation particles in each cell is set as 2000 and the maximum mass of the simulation particle is taken as $m_p = 1 \times 10^{-3}$. The averaged solutions of the last 10 000 iterations are output for comparison.

The density, u velocity, v velocity, and temperature contours for the test case of Kn = 0.1 obtained by different methods are compared in Fig. 16, and the comparison of the corresponding density, u velocity, pressure and temperature profiles along the stagnation line is depicted in Fig. 17. Basically, the results obtained by the DUGKWP compare well the those of the MDUGKS. Likewise, good agreements are achieved for the test case of Kn = 1, as shown in Figs. 18 and 19. In addition, the comparisons of the computational time and memory cost between the DUGKWP and the MDUGKS for simulating this test example are reported in Table II. The computational efficiency of the present scheme appears to be

TABLE II. Comparison of computational time (hr) and memory cost (MB) of different methods for flow around a circular cylinder at different Knudsen numbers.

	Scheme	Kn = 1	Kn = 0.1
Computational time	MDUGKS	43.89	38.28
	DUGKWP	4.51	2.71
	Time ratio	9.73	14.13
Memory cost	MDUGKS	8929	8929
	DUGKWP	807	807
	Memory ratio	11.06	11.06

nearly an order of magnitude higher than the MDUGKS with only about 1/11 memory consumption of the latter. These observations verify the excellent accuracy and efficiency of the DUGKWP for solving hypersonic rarefied flows.

V. CONCLUSIONS

Inspired by the idea of the UGKWP, a discrete unified gas-kinetic wave-particle (DUGKWP) method is developed in this work for the simulation of flows in all flow regimes. Like the UGKWP, the information on both microscopic particles and macroscopic flow variables is updated in the DUGKWP. Specifically, the microscopic particles are updated by the free-transport and resampling processes, and the macroscopic flow variables are evolved by the macroscopic governing equations. But different from the UGKWP, which is designed based on the local integral solution to the Boltzmann-BGK equation, the DUGKWP constructs from the local discrete characteristic solution to the Boltzmann-BGK equation. According to this local discrete characteristic solution, in the highly rarefied flow regime, the macroscopic fluxes are mainly attributed to the motion of microscopic particles, while in the continuum flow regime, the macroscopic fluxes are dominated by the macroscopic hydrodynamic waves. Analytical analysis indicates that the DUGKWP solves the collisionless Boltzmann equation in the collisionless limit and reduces to the N-S solver in the continuous limit, making it a multiscale approach.

Four test examples, including the Sod shock tube problem, the shock structure, the lid-driven cavity flow, and the hypersonic flow around a circular cylinder, are resolved to comprehensively evaluate the performance of the DUGKWP in all flow regimes. As compared with the deterministic approaches, such as the UGKS and MDUGKS, the DUGKWP method can provide accurate results in all flow regimes. For simulation of high-speed flows, the DUGKWP outperforms the MDUGKS in both computational efficiency and memory consumption. However, for simulation of low-speed flows, it is more efficient and has less memory consumption only when the flow goes to the continuum flow regime. As the Knudsen number increases, the statistical noise would disturb the solution, especially for low-speed flows. Overall, the DUGKWP is a multiscale method and appears to be a promising tool for modeling high-speed flows in a wide variety of flow regimes. Moreover, it is also expected to be applicable to the simulation of gas mixtures and plasma flow problems [46].

ACKNOWLEDGMENTS

The research is supported by the National Natural Science Foundation of China (Grants No. 12202191 and No. 92271103), Natural Science Foundation of Jiangsu Province (Grant No. BK20210273), Fund of Prospective Layout of Scientific Research for NUAA (Nanjing University of Aeronautics and Astronautics), and Priority Academic Program Development of Jiangsu Higher Education Institutions (PAPD).

[1] G. A. Bird, *Molecular Gas Dynamics and the Direct Simulation of Gas Flows* (Oxford University Press, London, 1994).

[2] J. Fan and C. Shen, Statistical simulation of low-speed rarefied gas flows, J. Comput. Phys. **167**, 393 (2001).

[3] Q. Sun and I. D. Boyd, A direct simulation method for subsonic, microscale gas flows, J. Comput. Phys. **179**, 400 (2002).

[4] T. J. Scanlon, E. Roohi, C. White, M. Darbandi, and J. M. Reese, An open source, parallel DSMC code for rarefied gas flows in arbitrary geometries, Comput. Fluids **39**, 2078 (2010).

[5] M. H. Gorji and P. Jenny, Fokker–Planck–DSMC algorithm for simulations of rarefied gas flows, J. Comput. Phys. **287**, 110 (2015).

[6] F. Fei, J. Zhang, J. Li, and Z. Liu, A unified stochastic particle Bhatnagar-Gross-Krook method for multiscale gas flows, J. Comput. Phys. **400**, 108972 (2020).

[7] L. Mieussens, Discrete velocity model and implicit scheme for the BGK equation of rarefied gas dynamics, Math. Models Methods Appl. Sci. **10**, 1121 (2000).

[8] V. A. Titarev, Conservative numerical methods for model kinetic equations, Comput. Fluids **36**, 1446 (2007).

[9] A. P. Peng, Z. H. Li, J. L. Wu, and X. Y. Jiang, Implicit gas-kinetic unified algorithm based on multi-block docking grid for multi-body reentry flows covering all flow regimes, J. Comput. Phys. **327**, 919 (2016).

[10] K. Xu, *A Unified Computational Fluid Dynamics Framework from Rarefied to Continuum Regimes* (Cambridge University Press, Cambridge, 2021).

[11] G. A. Bird, Shock-wave structure in a rigid sphere gas, in *Proceedings of the 4th International Symposium on Rarefied Gas Dynamics* (Academic Press, New York, 1965), Vol. 2, pp. 216–222.

[12] J. Moss, C. Glass, and F. Greene, DSMC simulations of Apollo capsule aerodynamics for hypersonic rarefied conditions, in *Proceedings of the 9th AIAA/ASME Joint Thermophysics and Heat Transfer Conference, San Francisco* (AIAA, Reston, VA, 2006), Paper No. AIAA 2006-3577.

[13] M. Fang, Z. H. Li, Z. H. Li, and C. X. Li, DSMC approach for rarefied air ionization during spacecraft reentry, Commun. Comput. Phys. **23**, 1167 (2018).

[14] D. B. Hash and H. A. Hassan, Assessment of schemes for coupling Monte Carlo and Navier-Stokes solution methods, J. Thermophys. Heat Transfer **10**, 242 (1996).

[15] T. E. Schwartzentruber, L. C. Scalabrin, and I. D. Boyd, Hybrid particle-continuum simulations of hypersonic flow over a hollow-cylinder-flare geometry, AIAA J. **46**, 2086 (2008).

[16] Z. Tang, B. He, and G. Cai, Investigation on a coupled Navier–Stokes–direct simulation Monte Carlo method for the simulation of plume flowfield of a conical nozzle, Int. J. Numer. Methods Fluids **76**, 95 (2014).

[17] F. L. Torre, S. Kenjeres, C. R. Kleijn, and J. L. P. A. Moerel, Evaluation of micronozzle performance through DSMC, in *Navier-Stokes and Coupled DSMC/Navier-Stokes Approaches//International Conference on Computational Science* (Springer, Berlin, 2009), pp. 675–684.

[18] P. L. Bhatnagar, E. P. Gross, and M. Krook, A model for collision processes in gases. I. Small amplitude processes in charged and neutral one-component systems, Phys. Rev. **94**, 511 (1954).

[19] E. M. Shakhov, Generalization of the Krook kinetic relaxation equation, Fluid Dyn. **3**, 95 (1968).
[20] J. E. Broadwell, Study of rarefied shear flow by the discrete velocity method, J. Fluid Mech. **19**, 401 (1964).
[21] J. Y. Yang and J. C. Huang, Rarefied flow computations using nonlinear model Boltzmann equations, J. Comput. Phys. **120**, 323 (1995).
[22] S. Chen, K. Xu, C. Lee, and Q. Cai, A unified gas kinetic scheme with moving mesh and velocity space adaptation, J. Comput. Phys. **231**, 6643 (2012).
[23] L. Mieussens, On the asymptotic preserving property of the unified gas kinetic scheme for the diffusion limit of linear kinetic models, J. Comput. Phys. **253**, 138 (2013).
[24] W. Su, L. Zhu, P. Wang, Y. Zhang, and L. Wu, Can we find steady-state solutions to multiscale rarefied gas flows within dozens of iterations? J. Comput. Phys. **407**, 109245 (2020).
[25] Z. H. Li and H. X. Zhang, Study on gas kinetic unified algorithm for flows from rarefied transition to continuum, J. Comput. Phys. **193**, 708 (2004).
[26] Z. H. Li and H. X. Zhang, Gas-kinetic numerical studies of three-dimensional complex flows on spacecraft re-entry, J. Comput. Phys. **228**, 1116 (2009).
[27] K. Xu and J. C. Huang, A unified gas-kinetic scheme for continuum and rarefied flows, J. Comput. Phys. **229**, 7747 (2010).
[28] Y. Zhu, C. Zhong, and K. Xu, An implicit unified gas-kinetic scheme for unsteady flow in all Knudsen regimes, J. Comput. Phys. **386**, 190 (2019).
[29] Z. Guo, K. Xu, and R. Wang, Discrete unified gas kinetic scheme for all Knudsen number flows: Low-speed isothermal case, Phys. Rev. E **88**, 033305 (2013).
[30] Z. Guo and K. Xu, Progress of discrete unified gas-kinetic scheme for multiscale flows, Adv. Aerodyn. **3**, 1 (2021).
[31] H. Liu, Y. Cao, Q. Chen, M. Kong, and L. Zheng, A conserved discrete unified gas kinetic scheme for microchannel gas flows in all flow regimes, Comput. Fluids **167**, 313 (2018).
[32] L. M. Yang, Z. Chen, C. Shu, W. M. Yang, J. Wu, and L. Q. Zhang, Improved fully implicit discrete-velocity method for efficient simulation of flows in all flow regimes, Phys. Rev. E **98**, 063313 (2018).
[33] L. M. Yang, C. Shu, W. M. Yang, and J. Wu, An improved three-dimensional implicit discrete velocity method on unstructured meshes for all Knudsen number flows, J. Comput. Phys. **396**, 738 (2019).
[34] C. Liu, Y. Zhu, and K. Xu, Unified gas-kinetic wave-particle methods I: Continuum and rarefied gas flow, J. Comput. Phys. **401**, 108977 (2020).
[35] Y. Zhu, C. Liu, C. Zhong, and K. Xu, Unified gas-kinetic wave-particle methods. II. Multiscale simulation on unstructured mesh, Phys. Fluids **31**, 067105 (2019).
[36] Y. Chen, Y. Zhu, and K. Xu, A three-dimensional unified gas-kinetic wave-particle solver for flow computation in all regimes, Phys. Fluids **32**, 096108 (2020).
[37] S. Liu, C. Zhong, and M. Fang, Simplified unified wave-particle method with quantified model-competition mechanism for numerical calculation of multiscale flows, Phys. Rev. E **102**, 013304 (2020).
[38] H. Liu, L. Quan, Q. Chen, S. Zhou, and Y. Cao, Discrete unified gas kinetic scheme for electrostatic plasma and its comparison with the particle-in-cell method, Phys. Rev. E **101**, 043307 (2020).
[39] J. Chen, S. Liu, Y. Wang, and C. Zhang, Conserved discrete unified gas-kinetic scheme with unstructured discrete velocity space, Phys. Rev. E **100**, 043305 (2019).
[40] K. Xu, M. Mao, and L. Tang, A multidimensional gas-kinetic BGK scheme for hypersonic viscous flow, J. Comput. Phys. **203**, 405 (2005).
[41] K. Xu, A gas-kinetic BGK scheme for the Navier–Stokes equations and its connection with artificial dissipation and Godunov method, J. Comput. Phys. **171**, 289 (2001).
[42] L. M. Yang, C. Shu, and J. Wu, Extension of lattice Boltzmann flux solver for simulation of 3D viscous compressible flows, Comput. Math. Appl. **71**, 2069 (2016).
[43] S. S. Kim, C. Kim, O. H. Rho, and S. K. Hong, Cures for the shock instability: Development of a shock-stable Roe scheme, J. Comput. Phys. **185**, 342 (2003).
[44] U. Ghia, K. N. Ghia, and C. T. Shin, High-Re solutions for incompressible flow using the Navier-Stokes equations and a multigrid method, J. Comput. Phys. **48**, 387 (1982).
[45] W. Liu, C. Shu, C. J. Teo, Z. Y. Yuan, Y. Y. Liu, and Z. L. Zhang, A simple hydrodynamic-particle method for supersonic rarefied flows, Phys. Fluids **34**, 057101 (2022).
[46] C. Liu and K. Xu, Unified gas-kinetic wave-particle methods IV: Multi-species gas mixture and plasma transport, Adv. Aerodyn. **3**, 1 (2021).